Title: An increase in the duration of an extended G1 period enables stochastic competition between terminal cell differentiation and cell-cycle re-entry

Authors: Michael L. Zhao[1], Atefeh Rabiee[1], Kyle M. Kovary[1], Zahra Bahrami-Nejad[1], Brooks Taylor[1], and Mary N. Teruel[1,*]

Affiliations:
[1]Dept. of Chemical and Systems Biology, Stanford University, Stanford, CA

***Corresponding Author:** mteruel@stanford.edu

SUMMARY

Terminal cell differentiation is essential for developing and maintaining tissues in all multi-cellular organisms and typically requires that proliferating progenitor cells exit the cell cycle. However, the relationship and timing between the underlying opposing processes, proliferation and terminal differentiation, is not yet understood. Using adipogenesis as a model system for terminal cell differentiation, we delineate the timing between cell-cycle exit and terminal differentiation by live-cell imaging of cell-cycle reporters and expression of PPARG, a master regulator of differentiation. We show that, during terminal cell differentiation, the levels of PPARG and of the CDK inhibitor p21 are coupled, and both gradually increase after mitosis. Expression of p21 regulates the duration of a variable extended G1 phase that allows some cells sufficient time to reach a PPARG threshold for differentiation instead of entering the next cell cycle when PPARG is again suppressed. By way of regulating the duration of an extended G1 phase during terminal differentiation, progenitor cells can stochastically control the number of final cell divisions and thus, the total number of differentiated cells.

HIGHLIGHTS

- Cells commit to differentiate by employing a stochastic competition process that typically occurs over multiple cell cycles during the extended G1 periods between mitosis and S-phase.
- Differentiation commitment occurs if the extended G1 duration is sufficiently long to allow PPARG levels, which increase at variable rates between cells in response to the differentiation stimulus, to reach a threshold that results in both irreversible differentiation and cell-cycle exit instead of the cells again entering the next S-phase and suppressing PPARG.
- The G1 cyclin-CDK inhibitor p21 is induced by PPARG and prolongs the extended G1 as well as triggers cell-cycle exit once PPARG reaches the threshold for differentiation.
- The underlying system architecture allows organisms to control tissue size by controlling the number of precursor cell divisions that occur before terminal differentiation.

Terminal differentiation typically requires that proliferative precursor cells transition into post-mitotic differentiated cells that are in a state of prolonged or permanent withdrawal from the cell cycle. In metazoans, failure of terminally differentiated cells to withdraw from the cell cycle affects the balance between the number of precursor and differentiated cells and can lead to cancer and metabolic disorders (Ghaben and Scherer, 2019; Ruijtenberg and van den Heuvel, 2016). An important early finding supporting a molecular link between differentiation and cell-cycle arrest showed that the muscle specific transcription factor, MyoD, upregulates the cyclin dependent kinase inhibitor, p21, to inhibit cell-cycle activity in a p53-independent manner (Guo et al., 1995; Halevy et al., 1995). Indeed, the link between p21 expression and terminal differentiation seems to be widespread across different terminally differentiated cells (Parker et al., 2006). It was also observed that lineage-specific transcription factors, such as CEBPA, have anti-mitotic activity that is independent of their transcriptional activity and that occurs possibly by inhibiting cyclin-CDKs (Harris et al., 2001; Umek et al., 1991). More recent work has supported roles for other CDK inhibitors, suggesting parallel inhibitory pathways, and identifying redundancy among regulators of cell-cycle exit in a tissue-specific manner (Buttitta et al., 2007; Ruijtenberg et al., 2015; Zalc et al., 2014). In the case of adipogenesis, regulation of CDK activity clearly plays a critical role in regulating differentiation as mice lacking the CDK inhibitors p21, p27, or both have up to 4 times higher fat mass (Naaz et al., 2004). Taken together, these prior studies establish a rich set of molecular connections between regulators of terminal differentiation and the control of cell-cycle exit.

However, the timing and order of these molecular connections is not understood, although these are essential parameters that need to be understood to control the terminal differentiation process. Since cell division and differentiation are asynchronous processes that occur on different timescales of hours versus days, it has been difficult to define the identity and order of events during the proliferation-differentiation decision. Interestingly, some terminal differentiation processes such as skin renewal, adipose tissue expansion, spermatogenesis, and development of the Drosophila eye have been reported to undergo a precise number of cell divisions before differentiation (Aragona et

al., 2017; Baonza and Freeman, 2005; Hsu et al., 2014; Insco et al., 2009; Tang et al., 2003), while others suggested more variable numbers of divisions (Clayton et al., 2007; Jones et al., 2007). These observations raise the following questions: does terminal differentiation occur stochastically in relationship to the cell cycle and what may be the underlying cause? Furthermore, when along the differentiation trajectory is the post-mitotic state established and how do cells coordinate cell cycle exit with the expression of regulators of terminal differentiation? A major obstacle to addressing these fundamental questions has been the inability to dynamically monitor terminal differentiation and cell cycle progression simultaneously in the same cell (Ruijtenberg and van den Heuvel, 2016).

A key tool that has been missing is a marker that can define the precise time when a cell irreversibly commits to the differentiated state. Many terminal cell differentiation systems including adipogenesis and myogenesis are regulated by a cascade of transcription factors (Blais et al., 2005; Farmer, 2006). In order to establish a temporal marker for commitment in any differentiation system, it is essential to determine which of the factors in the transcriptional cascade exhibits bimodal, and irreversible behavior and can thus be used to distinguish whether a cell will stay undifferentiated or terminally differentiate. For example, even though the early transcription factor CEBPB is required for adipogenesis, it is not a suitable marker of differentiation commitment. CEBPB levels increase in all cells that are subjected to the DMI adipogenic stimulus, but the levels are not predictive of whether or not a cell will continue on to differentiate once the stimulus is removed (Bahrami-Nejad et al., 2018). However, in previous work using single-cell imaging, we showed that the transcription factor PPARG exhibits bimodal, irreversible behavior and that a threshold level of PPARG can distinguish undifferentiated from differentiated cells (Ahrends et al., 2014; Bahrami-Nejad et al., 2018; Park et al., 2012) (Figure 1A-C).

Here using PPARG, we validate the concept that a threshold level in a transcription factor can mark in live cells the precise time when cells irreversibly commit to differentiate. By combining a live-cell endogenous PPARG sensor that can precisely mark the time of differentiation commitment with a widely used FUCCI cell-cycle sensor (Sakaue-Sawano et al., 2008), we establish for the first time a

method to track both cell-cycle progression and the decision to terminally differentiate simultaneouslsy in thousands of living single cells. Our live-cell experiments show that the irreversible commitment point for terminal differentiation occurs almost exclusively in an “extended G1” period which is a G0/G1 period between mitosis and S-phase that is variable in duration between cells. Normally the cell cycle suppresses PPARG expression during late G1, S, G2 and M phase through a CDK-regulated mechanism. However, adipogenic stimuli enable creation of an extended G1 period during which PPARG increases can occur. This creation of an extended G1-period is driven by PPARG-regulated expression of p21, a well-known regulator of G1-duration. If the extended G1 period is sufficiently long, cells are able to reach the PPARG commitment point, and cells are subsequently forced into permanent quiescence. If the extended G1 period is too short, cells start the next cell cycle first, and PPARG is again repressed until the next mitosis. We further show that a threshold in PPARG levels not only irreversibly commits cells, but also marks the point when p21 reaches a sufficiently high level to keep cells in a post-mitotic state.

We conclude that adipogenic stimuli generate an extended G1 period during which cells can compete after each mitosis between cell-cycle re-entry and terminal cell differentiation. Adipogenic stimuli control both the duration of the extended G1 and the rate of increase of PPARG after mitosis, thereby triggering a fraction of cells to differentiate during each of a few final division cycles. Thus, the adipogenic stimulus not only controls whether cells differentiate but also how many differentiated cells are generated per precursor cell. Finally, our finding of a competitive, stochastic nature of terminal differentiation out of a variable extended G1 phase highlights the critical need for live-cell tools and analysis methods in order to delineate the intricate order of events during the several-day long transition from proliferative precursors to post-mitotic differentiated cell states.

RESULTS

Measurement of the precise time when cells irreversibly commit to differentiate based on live single-cell analysis of the endogenous expression level of PPARG

A major bottleneck in understanding the relationship between exit from the cell cycle and irreversible commitment to the differentiated state has been the lack of a quantitative live-cell readout that can mark the point in time when differentiation commitment has occurred (Buttitta and Edgar, 2007). Thus, we first established a live-cell readout for cell differentiation using adipogenesis as a model system. We chose adipogenesis to study the proliferation-to-differentiation transition since previous studies have demonstrated in vitro and in vivo that adipogenesis is linked to cell division (Jeffery et al., 2015; Tang et al., 2003). Furthermore, adipogenesis has an added advantage as a model system in that it is a well-defined and experimentally accessible system (Ghaben and Scherer, 2019). Adipogenesis is centered around a master transcriptional regulator, PPARG, whose expression is driven by both input signals and positive-feedback loops (Ahrends et al., 2014; Rosen and Spiegelman, 2014) (Figure 1A). In previous work, we used CRISPR-mediated genome editing to fluorescently tag endogenous PPARG in preadipocyte cells as a live-cell readout of differentiation progression (Bahrami-Nejad et al., 2018). Here we validate the functional relevance and predictability of using a threshold level in PPARG to mark in live cells the point in time when an individual cell irreversibly commits to the terminally differentiated state.

To induce differentiation, we applied a commonly-used adipogenic hormone cocktail (DMI, see Methods) that mimics glucocorticoids and GPCR-signals that raise cAMP. Our experiments consisted of applying DMI for 48 hours to preadipocyte cells expressing endogenous fluorescently tagged PPARG (citrine-PPARG cells) and then removing the stimulus for 48 hours to test whether cells would continue on to the differentiated state independently of the stimulus (Figure 1B). Indeed even though the differentiation stimulus had been removed for 48 hours, one population of cells continued to increase PPARG levels due to engagement of CEBPA and other positive-feedback loops to PPARG (Figure 1B, blue traces) whereas the other population of cells either did not differentiate or did not increase PPARG levels sufficiently to reach the PPARG threshold and thus dropped back down to the undifferentiated state (Figure 1B, orange traces). At 96 hours, the PPARG levels of the cells was clearly bimodal with one peak representing the differentiated cells and the other the undifferentiated

cells (Figure 1B, right-side histogram).

To check for the existence of a PPARG threshold, we compared the PPARG levels at 48 hours just before the stimulus was removed to the PPARG levels at the 96-hour timepoint, 48-hours after the stimulus had been removed and cells had a chance to continue onto the differentiated state or drop back to the undifferentiated state. As shown in Figure 1C, the level of PPARG at 48 hours just before the stimulus was removed could predict whether cells would go onto a differentiated state even after the stimulus was removed. As different microscope parameters and cell culture conditions can change between experiments, the PPARG threshold value is calculated in each experiment from an analysis of the level of PPARG at the time the adipogenic (DMI) stimulus is removed, typically after 48 hours (see Methods section). Briefly, the PPARG distribution at 96 hours is first fit with a two-component Gaussian model that is used to classify whether a cell was differentiated or undifferentiated. The threshold is then calculated as the PPARG value at the 48-hour time point, just before the stimulus was removed, that can predict differentiated and undifferentiated cells with a less than 5% false positive rate (Figures 1B-C, black dashed line). High PPARG levels directly correlate with many commonly-used markers of differentiated adipocytes at the single-cell level (Figure 1D), consistent with the conclusion that citrine-PPARG levels going above the PPARG threshold marks an irreversible commitment point to differentiation.

To further define the properties of this citrine-PPARG commitment point, we estimated how predictable PPARG levels are for whether or not a cell will differentiate. Specifically, we asked how well a given level of PPARG at 24, 48 or 72 hours can predict the differentiation fate outcome at 96 hours, 48 hours after removal of the adipogenic stimuli (Figure 1E). We binned cells at the 3 timepoints according to their PPARG levels and plotted for each bin the fraction of cells that were above the PPARG threshold at the end of the experiment. The data takes the shape of a logistics curve and provides an estimate of the probability that a cell will differentiate at a given PPARG level. As shown in Figure 1E, cells will terminally differentiate more than 70% of the time when they reach the PPARG threshold level and close to 100% when PPARG levels increase another 50%. As a comparison, both

the integral and derivative values of PPARG changes served as poorer predictors of the final differentiated state (Figure S1). Interestingly, the probability of differentiation in cells did not exhibit a strong dependence on PPARG levels at the start of the experiment (Figure 1E), suggesting that the PPARG threshold represents a decision point that is generated in response to addition of a differentiation stimulus and is not just simply a predetermined feature of the cells.

Next, we investigated whether the PPARG threshold marks a qualitative change in PPARG dynamics as would be expected in a bistable system. We computationally aligned single cell traces by the time in which the cell crossed the threshold. This analysis shows that the threshold indeed marks a point where PPARG dynamics change from being stably low to stably high (Figure 1F). Analysis of the PPARG derivative around this threshold point also showed that the change occurred fast relative to the 96-hour time course, with a large increase in PPARG occurring in a 3-hour window around the threshold point (Figure S2A). Lastly, we found that PPARG levels were not correlated with endpoint measurements of adipocyte markers early in adipogenesis, but once the threshold was reached, PPARG levels sharply switched to being positively correlated (Figure 1G), supporting that the PPARG threshold marks a precise time when precursor cells commit to becoming mature fat cells and therefore defines a differentiation commitment point in single cells. Interestingly, by aligning PPARG timecourses by when the threshold was reached, we are able to measure a distinct time when differentiation markers strongly correlate with PPARG levels and differentiation commitment occurs. However, if we had not been able to calculate and define a PPARG threshold and we were thus unable to align the timecourses, we would only see that there is an increased relationship between PPARG expression and mature adipocyte markers; for example, see rightmost plot in Figure 1G which shows a gradual increase in correlation with PPARG with GLUT4 when timecourses are not aligned by the threshold. Thus, without being able to measure a threshold for each cell and being able to align the PPARG timecourse for each cell by this threshold, we would be unable to mark a precise timepoint for differentiation commitment, as is obvious in the other plots in Figure 1G.

Development of a system to measure terminal differentiation and cell division at the single-cell level

To measure cell cycle and differentiation progression simultaneously in the same cells, we made a dual-reporter cell line by transfecting a FUCCI cell-cycle reporter (Sakaue-Sawano et al., 2008) into OP9 preadipocyte cells expressing endogenous citrine-PPARG (Figure 2A). The cell-cycle reporter is composed of a fragment of the geminin protein fused to the red fluorescent protein mCherry, and its nuclear-localized fluorescent signal is dependent on the activity of the anaphase promoting complex/cyclosome (APC/C^{Cdh1})(Cappell et al., 2016). When APC/C^{Cdh1} activity is turned off near the G1-to-S phase transition, the geminin degron sensor begins to accumulate to high levels, thus marking re-entry into the cell cycle. When APC/C^{Cdh1} becomes active during anaphase of mitosis, the sensor is rapidly degraded, and the fluorescence drops to near background levels. The cells were also stably transfected with fluorescently-labeled H2B to enable automated nuclear tracking as cells move during differentiation. Differentiation experiments were performed under subconfluent conditions such that most cells could undergo multiple divisions with minimal contact with other cells. These conditions yielded 20-50% differentiated cells after a typical 96-hour DMI differentiation protocol compared to ~80% differentiated cells under more confluent conditions (Figure S3). We chose these conditions to maximize the number of cell divisions, reduce the effect of cell density on cell cycle arrest, and improve fidelity of the automated tracking algorithm by reducing cell crossover events. Our dual-reporter cells allow us to visualize cell-cycle and differentiation progression simultaneously in thousands of single living cells and to quantitatively measure parameters such as the number of division events, differentiation state, and the duration of the G1 phase between mitosis and S-phase, all in the same cell (Figures 2A-C).

Supporting an inverse relationship between proliferation and differentiation, cells that stayed cycling longer remained undifferentiated, and cells that differentiated underwent fewer mitoses (Figures 2B-C). Furthermore, plotting the dual-reporter timecourses in individual cells clearly showed that no proliferation is observed after cells commit to differentiation and that PPARG typically fails to

increase if cells are proliferating (Figure 2D). In cells that differentiate, the PPARG increase to the threshold is typically only observed after the end of the last mitosis, supporting that the cell cycle largely suppresses differentiation during the S/G2/M phases. We carried out experiments to confirm that the cell-cycle suppression of differentiation was likely due to an active cellular control mechanism and not simply due to dilution of PPARG resulting from additional cell divisions (Figure S4). Mechanistically, the reason why dilution of PPARG is unlikely to contribute to the decrease in differentiation in cycling cells is the very short half-lives of PPARG of both the protein and mRNA of ~1 hour (Bahrami-Nejad et al., 2018), arguing that the concentration of PPARG remains largely the same when a cell divides and grows its protein mass.

A histogram of the difference in time between the end of the last mitosis and when a cell reaches the PPARG threshold shows that if a cell differentiates, it does so only after an average delay of approximately 14 hours after the last mitosis is completed (Figure 2E). That the decision to renter the cell cycle or to differentiate happens during the G1 phase after mitosis was also shown by differentiating and analyzing cells stably transfected with a CDK2 reporter (Spencer et al., 2013)(Figure 2F). CDK2 activity starts to increase in G1 phase and increases gradually until mitosis when it drops back to basal levels at anaphase before the two daughter cells are born. Markedly, timecourse analysis of the CDK2 reporter in differentiating preadipocyte cells showed that the PPARG threshold is reached almost exclusively in G1, when the geminin-based reporter is still suppressed and before CDK2 activity levels increase. The generality of this observation is confirmed by a scatter plot analysis of hundreds of cells at all time points during differentiation which shows that PPARG levels are high only when CDK2 activity levels are low (Figure 2G).

Notably, there is a variable number of mitoses that cells undergo before differentiating (Figure 2C-D), supporting that terminal cell differentiation of adipocytes does not occur by a fixed number of cell divisions before differentiation as has been previously reported (Tang et al., 2003). The previous study may not have identified such variable numbers of mitoses before differentiation because it relied on averaged, population-based measurements and could not resolve cell-to-cell differences in mitoses

numbers as is possible with the live single-cell imaging approach of the current study. It is also apparent from the timecourses in Figure 2D that there is great variability in the time after stimulation when cells start to increase PPARG levels and also in how long after the last mitosis cells spend in the G1-period before reaching the PPARG threshold.

Adipogenic stimuli result in a gradual increase in G1 phase duration and a decrease in time to reach the PPARG threshold for differentiation after mitosis

Our timecourse data thus far shows that PPARG increases to the differentiation commitment point primarily only in G1 phase. Since PPARG expression is suppressed during S/G2/M, this argues that there is a competitive race during each G1 phase between whether a cell can build PPARG levels up fast enough to reach the commitment point to irreversibly differentiate or whether the cell re-enters the next cell cycle and PPARG levels are again suppressed. But how can cells ever win the race to differentiate when G1 duration in proliferating cells is typically only approximately 4 hours whereas a cell typically needs on the order of days in G1 phase for PPARG levels to build up to the threshold (Figure 3A)? It should be noted that a slow increase of a key differentiation regulator to an irreversible differentiation commitment point, such as occurs with PPARG during adipogenesis, could be a desired feature of differentiation systems since it enables cells to reject transient differentiation signals (Bahrami-Nejad et al., 2018).

To answer this question, we determined whether G1 duration changes during the differentiation process. In cells that underwent three observed mitoses before differentiating, we compared the G1 duration for the first and second observed G1 phases ($G1_1$ and $G1_2$, see scheme in Figure 3B). Strikingly the duration of G1 increases the longer a cell is subjected to the adipogenic stimulus (Figure 3C). Particularly, the duration of G1 increases strongly once the differentiation stimulus is applied for 24 hours or longer (Figure 3D). This time is also when positive feedback loops to PPARG typically start to engage (Bahrami-Nejad et al., 2018), suggesting that an important role of adipogenic stimuli is to generate the extended G1 period. As described earlier, we here use the term

“extended G1” to describe the variable, often much longer, G1 period between mitosis and S phase that extends beyond the typical minimal G1 duration of about 4 hours in proliferating preadipocytes (Figure 3A).

We next used the natural variation in our data to ask whether an extended G1 duration could be beneficial for differentiation. We used the timecourse data shown in Figure 2B and binned cells into groups based on when a cell completed its last mitosis in increments of 4 hours (see scheme in Figure 3E). We first plotted two properties of the bins: 1) the fraction of cells that were differentiated at 96 hours in that bin (y-axis, % PPARG high cells) and 2) the average time the cells in that bin spent in G1 before reaching the differentiation threshold (x-axis). Indeed, we observed a positive correlation between the ability of cells to differentiate and the time they spent in the extended G1 (Figure 3F, left). We also observed that the later a cell exited the cell cycle, and thus the longer the proliferating cell was exposed to the adipogenic stimuli, the less time that cell needed to spend in G1 before reaching the PPARG threshold (Figure 3F, right).

The timecourses in Figure 2D show that the cell cycle initially suppresses PPARG increases and differentiation during the S/G2/M phases. However, by computationally aligning the timecourses by the time each individual cell completed its last mitosis, we can more precisely measure PPARG increases before and after the last mitosis (Figure 3G). If a cell has a last mitosis in the first 12 hours after DMI addition, PPARG does not increase noticeably both before or within 12 hours after mitosis. However, if a cell has its last mitosis 12-24 hours after DMI addition, PPARG shows a small increase starting already within approximately 4 hours after mitosis. This increase becomes much stronger when a cell has its last mitosis 24-36 hours after DMI addition, and a small increase in PPARG can also be observed before the end of the last mitosis. If a cell has its last mitosis 36-48 hours after DMI addition, it is apparent that PPARG can increase significantly even before mitosis is over, suggesting that exposure to the adipogenic stimulus helps to overcome the cell-cycle suppression of PPARG and thereby facilitates cells reaching the PPARG threshold after mitosis. Note that the spike in in the PPARG levels at aligned timepoint 0 is due to aligning the timecourses to mitosis. At this timepoint,

there is an undefined nuclear PPARG signal because the nuclear envelope is broken down and chromatin (H2B) is condensed. As shown in Figure 3H, the cells that went on to differentiate were able to partially overcome the cell cycle suppression of adipogenesis and to increase their PPARG levels already before the end of the last mitosis.

The cell cycle in progenitor cells operates on the timescale of several hours whereas differentiation commitment occurs on the timescale of days (Figure 3A). This raises the question how two processes with such different timescales can influence each other. Proliferating cells typically exhibit a suppressed increase of PPARG expression and a failure to differentiate every time they cycle through S/G2/M (i.e., Figure 2B-D). However, the differentiation process has a chance to overcome this cell cycle suppression at the end of each mitosis in G1, the phase during which cells reach the threshold for differentiation with increasing likelihood, and before re-entering the next S/G2/M cycle. Our live-cell timecourses show that there is a great deal of variability between cells in how long the G1 period is and how fast PPARG levels rise after mitosis. As depicted in Figure 3I, if the G1 period is too short in duration and the rate of PPARG increase is too slow to reach the threshold to differentiate, cells will re-enter the cell cycle and the subsequent S/G2/M phases will once again suppress PPARG expression. However, if the differentiation stimuli can cause PPARG to rise fast enough and G1 phase is extended long enough, cells are able to reach the threshold for differentiation and in turn suppress proliferation to enter into a post-mitotic state. Our results in Figure 3 argue that differentiation stimuli help in two ways to overcome the cell cycle suppression of differentiation: 1) by increasing the rate at which PPARG increases to the threshold after mitosis and 2) by increasing the duration of an extended G1 phase. Thus, differentiation stimuli control not only whether precursor cells differentiate but also how many cell cycles there are in response to adipogenic stimulation, and as a consequence, how many differentiated cells are produced per precursor cells. Notably, there are also always some cells in a population stimulated with adipogenic stimuli that remain undifferentiated in a prolonged G1 state (Figures 2D and 3F). The mechanism for extending G1 is likely stronger in these cells than the upregulation of the differentiation program which means that they stop dividing but

cannot sufficiently upregulate PPARG.

The CDK inhibitor p21 and cyclin D1, which both regulate the duration of G1 phase, antagonistically regulate the number of differentiating cells

We next focused on understanding the mechanistic basis for the observed correlation between G1 duration and terminal cell differentiation. We first carried out experiments to explore the role of p21, a protein which is known to control cell-cycle re-entry after mitosis (Yang et al., 2017). We found that knockdown of p21 decreased G1 duration, as measured by the integrated total time spent in G1 in 96 hours (Figure 4A, left). This decrease in G1 duration was associated with an increase in the fraction of cycling cells (Figure 4A, middle) and a decrease in terminal differentiation over time as monitored by lower average PPARG expression (Figure 4A, right). Conversely, increasing expression of human p21 using a DHFR induction system yielded the opposite effect: the fraction of cycling cells decreased and there was a corresponding small increase in average PPARG expression (Figure 4B). Since the D-type cyclins are also known to regulate the duration of G1, but in opposite fashion compared to p21 (Yang et al., 2017), we next tested the effect of reducing cyclin D1 expression on the proliferation-differentiation switch. Consistent with our model of an extended G1 phase controlling whether a cell commits to differentiate, we found that cyclin D1 knockdown led to an increase in G1 duration, a decrease in cell-cycle activity and again a corresponding increase in differentiation (Figure 4C). Furthermore, our results showing that knockdown of cyclin D1 both prevented further entry into S-phase in most cells and caused a premature increase in PPARG levels support that PPARG increases are suppressed during S/G2/M phases, as was indicated from the timecourses in Figure 2D. Our results do not exclude the possibility that cyclin Ds have additional roles in regulating differentiation that do not work through regulation of CDK4/6 (Fu et al., 2005). Our findings are consistent with the interpretation that cyclin D1 and p21 have opposing roles in controlling the duration of the extended G1 period and thereby have opposing roles in controlling differentiation outcome.

We next tested whether regulators of G1, such as growth factors that regulate cyclin D1, could

also regulate the degree of differentiation. To decrease growth factor signaling activity, we lowered the fetal bovine serum (FBS) concentration in the cell media from 10% to 2% or added a MEK inhibitor in the differentiation cocktail to inhibit the Ras/MEK/ERK pathway known to upregulate cyclin D1. Both conditions resulted in a decrease in cell-cycle activity and a concomitant increase in differentiation (Figure 4D, top panels). Interestingly, when we added a large concentration of EGF back into the 2% FBS condition, the cells differentiated to the same degree as observed in the 10% FBS condition but did not re-enter the cell cycle in the same manner as observed in 10% FBS differentiation media (Figure 4D, bottom panels). This suggests that the effect of growth factors on differentiation is in part caused by their effect on proliferation but also through additional mechanisms. Together, these experiments validate our observation that G1 duration and differentiation are closely connected and further show that the response to growth factors affects the decision to proliferate or differentiate. Our combined experiments show how the decision to proliferate and differentiate mutually oppose each other during an extended G1 and are both regulated by adipogenic, as well as growth factor, stimuli.

PPARG controls cell-cycle activity in part by upregulating p21 expression

We next investigated how PPARG levels regulate the cell cycle before and after the differentiation commitment point. We had previously observed over the course of a typical differentiation experiment that cells which continuously proliferate are strongly correlated with persistently low levels of PPARG (Figure 2B). We now validated this observation by using RNA interference against PPARG. We found that depletion of PPARG indeed increased the fraction of proliferating cells throughout the entire time course of the experiment (Figure 5A). Based on our observation that differentiation commitment occurs in a state with low CDK2 activity and previous work identifying p21 as a major regulator of cells in the CDK2 low state, we hypothesized that CDK inhibitors in general may play a critical role in inhibiting cell division during adipogenesis in our cells. We performed RNA-sequencing on cells transfected with siRNA targeting PPARG or non-targeting siRNA and collected at different timepoints during a 144-hour DMI differentiation protocol. We examined the

mRNA expression profiles of all canonical CDK inhibitors and identified two that were strongly regulated by PPARG expression, p18 and p21 (Figure 5B). To validate that p18 and p21 could mediate cell-cycle arrest during adipogenesis, we carried out siRNA knockdown experiments and found that p21, but not p18, knockdown led to an increase in cell divisions under differentiation conditions (Figure 5C).

Our results support that p21 can be upregulated transcriptionally by PPARG in preadipocyte cells (Figure 5B), as has been demonstrated in other cell types (Han et al., 2004). We also explored additional potential mechanisms which could upregulate p21 during adipogenesis. The RNA-seq dataset also showed that FKBPL (WiSP39) was upregulated throughout differentiation in a PPARG-dependent manner (Figure 5D). FKBPL has previously been shown to stabilize p21 and increase its ability to arrest cells in response to ionizing radiation (Jascur et al., 2005). To test if a similar mechanism could function during the early stages of differentiation, we carried out cycloheximide protein degradation experiments to measure the half-life of p21 in cells transfected with siRNA targeting FKBPL or a control. Our results showed that knockdown of FKBPL decreased p21 half-life but did not affect the half-life of PPARG, supporting that FKBPL does regulate p21 stability during terminal cell differentiation (Figure 5E). Lastly, we tested whether adding a direct activator of PPARG could also upregulate p21 expression. Indeed, the addition of rosiglitazone led to a robust increase in p21 expression (Figure 5F). Taken together, our results suggest that PPARG arrests the cell cycle in part through the regulation of p21 levels by both transcriptional and post-transcriptional mechanisms. In further support of the result of Figure 4D that regulation of p21 may have a more pronounced role compared cyclin D1 in regulating G1-period duration and adipogenesis, the levels of cyclin D1 did not change significantly when adipogenic stimuli were applied whereas p21 levels did change significantly (Figure S5). Taken together, our results identify a rate-limiting molecular mechanism controlling the active competition between proliferation and differentiation that is restricted to an extended G1 phase (Figure 5G). The competition starts with a small increase in PPARG, that in some cases already starts in mother cells, which promotes upregulation of p21 to suppress re-engagement of CDK2 activity

during G1 and thereby allow cells to generate an extended G1 period so that cells have sufficient time to increase PPARG levels and reach the differentiation commitment point. The observed suppression of PPARG expression (e.g. Figure 2D) is likely mediated by a previously described induction of E2F-target genes such as UHFR1 or E2F itself (Fajas et al., 2002; Sabatino et al., 2012) that can inhibit PPARG expression. The lack of suppression of PPARG expression in G1 is then a consequence of E2F target genes being off during the extended G1 period and E2F-induction engaging each time when CDK is activated during the S/G2/M phases of the cell cycle.

Cells crossing the PPARG threshold for differentiation become unresponsive to mitogenic stimulation and are locked into a post-mitotic state by p21

To observe how the population of differentiating cells stopped cycling and reached the threshold to differentiate, we applied the standard 96-hour DMI protocol to induce adipogenesis of OP9 preadipocytes and plotted at each timepoint the percent of proliferating cells versus the percent of cells that crossed the differentiation commitment point. As shown in Figure 6A, initially cells were only proliferating, and no differentiation was observed. Subsequently, there was a time window from about 24-50 hours where both proliferation and differentiation were observed in an inverse relationship with the percent of cycling cells decreasing as cells enter the differentiated state. Finally, around 50 hours, the cell population was made up almost exclusively of differentiated cells that have exited from the cell cycle, as would be expected since adipocytes are known to be in a post-mitotic state. This raises the question how a terminally differentiating cell can enter into and maintain this irreversible exit from the cell cycle.

The typical differentiation protocol involves adding adipogenic stimuli for 48 hours and then replacing the media with fresh growth media and insulin for another 48 hours. We took advantage of this protocol in order to test how the level of PPARG in a cell would influence its ability to proliferate. Dual-reporter cells were stimulated to differentiate with the standard DMI protocol, and the relationship between PPARG levels and cell-cycle progression in response to media replacement at 48 hours was

measured by imaging citrine-PPARG and geminin levels (Figure 6B). Cells were then separated into 10 equal bins based on their PPARG levels at the 48-hour timepoint, one frame before the media was changed from DMI to media with just insulin and growth factors. The corresponding mean PPARG (left) and geminin-degron (right) signals were plotted for each bin. We found that the group of cells that passed the PPARG threshold showed no geminin response to fresh growth media. We confirmed that this represented reduced cell-cycle activity by calculating the fraction of cells that underwent mitosis, as assessed by the splitting of H2B during anaphase, in response to fresh growth media (Figure 6C, grey). Our finding that cells past the PPARG threshold had almost no response to freshly-added growth factors supports that crossing the PPARG threshold indeed marks a transition when cells lose the ability to enter the cell cycle and therefore have entered a post-mitotic state.

We had shown that p21 has a critical role in creating an extended G1 period (Figures 4 and 5). We therefore determined whether p21 is also responsible for maintaining the postmitotic state after cells have passed the commitment point to differentiate. After completion of a live cell time course, we fixed and stained cells for p21 expression. We again binned cells according to PPARG levels and plotted the mean nuclear p21 fluorescence for each bin (Figure 6C, black). We found a steady increase in p21 levels all the way through the PPARG threshold until it reached maximal levels after the PPARG threshold. Next, we transfected siRNA targeting p21, CEBPA, and PPARG late in adipogenesis at the 48-hour timepoint when the adipogenic stimulus was removed and replaced with media. CEBPA is a required co-activator of PPARG expression for cells to reach the threshold for differentiation (Bahrami-Nejad et al., 2018; Wu et al., 1999). These acute knockdowns after the commitment point showed that only p21 knockdown resulted in a dramatic increase in cell-cycle activity after cells had exceeded the PPARG threshold for differentiation (Figure 6D). Using the same data set, we binned cells by their PPARG levels and quantified the average response of each bin to freshly-added growth factors. Strikingly, knockdown of p21 expression led to a near complete loss of the ability of PPARG levels to control of cell-cycle exit, as illustrated by comparing the highest bins of PPARG-expressing cells which blocked cell-cycle activity when non-targeting siRNA was transfected but could no longer block cell-

cycle activity when p21 was knocked out (Figure 6E). As shown in Figure 6F, when p21 is present, the cell cycle is repressed in most cells above the PPARG threshold. However, when p21 is depleted, this ability to maintain a post-mitotic state in cells past the PPARG threshold is lost.

Notably, when we examined images of cells from Figures 6E-F, we found that PPARG high cells were enriched for multinucleation events (Figure 6G). This suggests that while a main role of p21 in PPARG high cells is to control the duration of the extended G1 period, another critical role is to continuously prevent cell division after differentiation to prevent mitotic defects. Finally, it was recently shown that the p21-cyclinD1 ratio can be a critical parameter controlling the G1/S transition (Yang et al., 2017). We explored whether a main role of p21 was to shift this p21-cyclinD1 ratio towards p21 to ensure that cells remain unresponsive to serum stimulation. As shown when p21 and cyclinD1 levels in the same single cells are plotted (Figure 6H), the ratio of p21 to cyclinD1 becomes dramatically skewed towards p21 when PPARG levels go above the threshold during adipogenesis, providing an explanation of how differentiated cells can maintain such a robust arrested state. Taken together, our data shows that the commitment to differentiation also marks the entry into a long-term post-mitotic state and that p21 is critically needed to maintain the postmitotic state after commitment.

DISCUSSION

Using adipogenesis as a model system, we carried out live-cell analysis to determine the molecular mechanisms and timing between cell-cycle exit and terminal differentiation. We show that the decision to terminally differentiate in cells subjected to an adipogenic stimuli is made out of an extended G1 phase after cells exit mitosis. Unexpectedly, the duration of the extended G1 phase varies between cells, and the average duration of this extended G1 increases as cells undergo one or more cell cycles following adipogenic stimulation. Furthermore, we found that expression of PPARG is repressed during S, G2, and M and starts to significantly increase during each extended G1 after mitosis. The rate of PPARG increase after mitosis varies between cells but becomes faster on average the later mitosis occurs following adipogenic stimulation.

We further showed that PPARG has to reach a critical threshold level before the end of the extended G1 period in order for cells to irreversibly commit to differentiate. Only when a cell reaches the PPARG threshold will multiple positive feedbacks engage that not only prevent the cell from returning to the undifferentiated state, but also suppress entry into the next cell cycle. However, if a cell reaches the end of the extended G1 phase before it reaches the PPARG threshold, the cell will enter the next cell cycle and suppress both the increase in PPARG and differentiation until the next mitosis. Thus, our data argues for a stochastic competition between proliferation and differentiation that occurs in a dedicated extended G1 window after mitosis. The role of adipogenic stimuli is to both increase the rate at which PPARG increases after mitosis and also extend the duration of the G1-phase. Mechanistically, we found that the CDK inhibitor p21, along with cyclin D1, has a critical rate-limiting role in defining the duration of the extended G1. The level of p21 is highly variable between cells (Figure 6H), explaining the observed variation in the extended G1 phase. When cells reach the PPARG threshold for irreversible differentiation, p21 plays a second critical role to maintain the postmitotic state. We showed that forced suppression of p21 after cells have passed the threshold for terminal differentiation can re-activate the cell cycle and trigger mitotic defects, arguing that p21 mediates the precise timing between differentiation and terminal cell-cycle exit which is critical for cell health. Our studies were performed at low cell density, and at higher cell densities the homolog CDK inhibitor p27 likely has a synergistic role along with p21 in regulating the duration of the extended G1. Such a synergistic role of both CDK inhibitors is consistent with knockout data in mice which showed a 6-fold increase in fat mass when p27 and p21 where knocked out together as compared to the individual knockouts (Naaz et al., 2004).

Our findings suggest that terminal differentiation is a stochastic transition that occurs over one or more cell cycles and that the final commitment point occurs during an extended G1 period. As shown in the model depicted in Figure 7A, in the initial cell expansion phase, the extended G1 is short, and proliferative precursors choose cell-cycle entry over differentiation largely independently of the differentiation stimulus. As the extended G1 becomes longer and the rate of PPARG expression after

mitosis begins to increase during the intermediate phase that occurs around 24 hours after adipogenic stimulation, a competition occurs in each cell after each mitosis as to whether PPARG levels reach the commitment point for differentiation or whether cells reenters the next cell cycle and PPARG expression is again repressed in the S/G/M2 phases. This competition is based on differentiation stimuli both gradually extending the G1 period (Figure 3B-D) and accelerating the rate of PPARG increase after mitosis (Figure 3E-G). In a third phase that starts during this extended G1, cells that have reached the commitment point for differentiation also continuously repress any further cell-cycle entry (Figure 2D). A fraction of cells can also be observed that initially proliferate but then stop dividing without differentiating (Figures 2D and 7B).

Given that tissues typically have fixed numbers of precursor cells, our results suggest that organisms can regulate differentiation in two ways. First, by changing the amplitude of adipogenic stimuli, different fractions of precursor cells with different sensitivity to adipogenic stimuli can be engaged and end up differentiating (Ahrends et al., 2014; Park et al., 2012). Second, dependent on the competition between proliferation and differentiation in the extended G1, cells stimulated to differentiate do not immediately differentiate but only do so on average after some 1, 2 or 3 cell cycles to generate per precursor cell 2, 4 or 8 differentiated cells, respectively (Figure 7B). Thus, our study argues that a functional consequence of a system with a regulated extended G1 is that organisms can control not only whether or not precursor cells differentiate but also how many differentiated cells are generated per precursor cell by having a longer or shorter initial proliferating phase that is regulated by both growth factor and differentiation stimuli. The dramatic effect of p21 and p27 inhibitor knockouts on fat mass (Naaz et al., 2004), and the role of p21 in regulating the extended G1 phase shown here, provide support for the hypothesis that the control of the duration of the extended G1 is a key mechanism controlling tissue size.

We conclude that terminal differentiation is closely intertwined with proliferation and that an extended G1 phase after mitosis establishes a critical time window during which competition between the differentiation program and next cell-cycle program can take place. We show that the competition

between proliferation and differentiation is in part based on PPARG promoting p21 expression and on cell-cycle progression during S/G2/M repressing PPARG, likely through E2F-dependent and E2F-independent mechanisms (Fu et al., 2005; Zaragoza et al., 2010). Our study shows several advantages of studying terminal differentiation in adipocytes as we were able to develop a live molecular marker to precisely determine when cells make the transition to the irreversible differentiated state. Our findings on the roles of CDK inhibitors in regulating an extended G1, together with terminal cell differentiation results from different knockout studies in vivo (Lange et al., 2009; Naaz et al., 2004), suggest that many terminal differentiation systems may rely on a stochastic competition process in an extended G1 phase during which cells either reach the threshold for differentiation and suppress proliferation or start the next cell cycle and suppress differentiation. Furthermore, our results provide mechanistic support for the hypothesis that tissue size and renewal are not only controlled by whether a precursor cell differentiates or not, but also by regulating the duration of the extended G1 which controls how many differentiated cells are generated per precursor cell.

METHODS

Generation of PPARG/geminin dual-reporter cell line.

OP9 cells with endogenously tagged citrine-PPARG2 and stably infected H2B-mTurqoise was generated as previously(Bahrami-Nejad et al., 2018) . Lentivirus was generated for the geminin degron reporter from the vector pCSII-EF-Geminin(1-110)-mCherry. A third-generation lentiviral packaging system was used and consisted of the following packaging vectors: pMDlg, pCMV-VSVG, and pRSV-Rev. The geminin reporter was then stably infected into H2B-mTurqoise/citrine-PPARG2 cells to generate the dual-reporter cell lines. Selection of dual-reporter cells was done with FACS for mCherry-positive cells.

Generation of PPARG/geminin/CDK2 triple reporter cell line.

Lentivirus was generated for the CDK2 sensor from the vector pCSII-EF-DHB-mTurquoise (gift from the lab of Tobias Meyer) in the same manner described above. Selection of triple-reporter cells was done with FACS for cells that were positive for both mCherry and mTurquoise.

Cell culture and differentiation.

Wildtype, dual-reporter, and triple reporter OP9 cell lines were cultured according to previously published protocols (Ahrends et al., 2014; Bahrami-Nejad et al., 2018; Wolins et al., 2006). The cells were cultured in growth media consisting of MEM-α media (ThermoFisher Scientific) containing 100 units/mL Penicillin, 100mg/mL Streptomycin, and 292 mg/mL L-glutamate supplemented with 20% FBS. To induce differentiation, two methods were used. In the first method, a standard DMI cocktail was used: cells were treated with 125 μM IBMX (Sigma-Aldrich), 1 μM dexamethasone (Sigma-Aldrich), and 1.75 nM insulin (Sigma-Aldrich) for 48h, followed by 1.75 nM insulin for 48h. In the second method, cells were treated with 1 μM of Rosiglitazone (Cayman, USA) for 48 hours, followed by 1.75 nM insulin for another 48 hours. For fixed cell experiments, the differentiation stimuli were added to the growth media described above with one modification: 10% FBS was used (instead of 20% FBS) during differentiation conditions. The one exception is in in the reduced serum experiments in Figure 4D, in which 2% FBS was used in the growth media during differentiation. For all live cell experiments, the differentiation stimuli were added to Fluorobrite DMEM media (ThermoFisher Scientific) containing 100 units/mL Penicillin, 100mg/mL Streptomycin, and 292 mg/mL L-glutamate supplemented with 10% FBS. For Figure 4D, EGF (Sigma-Aldrich E9644) was used at a final concentration of 1 μg/mL, and a MEK inhibitor PD0325091 was used at a final concentration of 100 nM.

siRNA-mediated gene silencing.

siRNA targeting *Pparg, Cebpa, p21, CyclinD1, Fkbpl* and the AllStars Negative Control siRNA were purchased from QIAGEN. For siRNA knockdown in the live-cell imaging experiments in dual-reporter cells (Figure 4, Figures 5a, 5d, and 5e), OP9 cells were transfected by reverse-transfection using μL Lipofectamine RNAiMax (Invitrogen). Briefly, our reverse-transfection protocol per well is as follows: mixed 20 μL of Optimem, 0.5 μL of a 10 μM siRNA stock solution, and 0.3 μL of RNAiMax. Let solution incubate at room temperature for 10 minutes and then add 80 μL of culture media containing the desired number of cells per well. Then the entire (~100μL) volume is plated into one well of a 96-well plate. The siRNA/RNAiMax mixture was left on the cells for 24 hours before being aspirated away and replaced with fresh culture media containing DMI to begin the differentiation protocol.

For the live-cell imaging experiments in dual-reporter cells transfected at the 48-hour timepoint (Figure 6), the following protocol per well was used: siRNA mixture was prepared using 0.6 μL Lipofectamine RNAiMAX, 0.5 μL of a 10 μM siRNA stock solution, and 20 μL of Optimem. Incubate the mixture for 10 minutes then add 180 μL of Fluorobrite media consisting of 1.75 nM insulin. The entire solution (~200μL total volume) was then added to cells at the 48-hour time point and left on until the end of the experiment.

Overexpression of p21

A retroviral vector containing DHFR-Chy-p21(Spencer et al., 2013) (gift from the lab of Tobias Meyer) was used to generate viral particles to stably infect DHFR-Chy-p21into a modified dual-reporter cell line. This cell line was also stably infected with H2B-iRFP670 and a version of the geminin degron fused to mCerulean3. Positive clones were selected for by FACS in cell culture media containing 10 μM TMP. Cells were sorted into culture media with no TMP and grown in the absence of TMP. All overexpression experiments were done by adding 10 μM TMP into the culture media or differentiation media. In control experiments, 10 μM DMSO was added instead of TMP.

Immunofluorescence (IF) staining

All cultured cells were fixed with 4% PFA in PBS for 30 min at room temperature, followed by five washes with PBS using an automated plate washer (Biotek). Cells were then permeabilized with 0.1% Triton X-100 in PBS for 15 minutes at 4°C, followed by blocking for 1 hour in 5% bovine serum albumin (BSA, Sigma Aldrich) in PBS. The cells were incubated with primary antibodies in 2% BSA in PBS overnight at 4°C: mouse anti-PPARγ (Santa Cruz Biotech, sc-7273, 1:1,000), rabbit anti-CEBPα (Santa Cruz Biotech, sc-61, 1:1,000), mouse anti-p21 (Santa Cruz Biotech, sc-6246, 1:100), cyclinD1

(Abcam, ab137145,1:1,000), adiponectin (Abcam, ab22554, 1:1,000), Glut4 (Santa Cruz Biotech, sc-1608,1:500), FABP4 (R&D Systems, AF1443, 1:1,000). After washing, cells were incubated with Hoechst (1:20,000) and secondary antibodies in 2% BSA / PBS for 1 hour. Secondary antibodies included AlexaFluor-conjugated anti-rabbit, anti-mouse , and anti-goat antibodies (Thermo Fisher Scientific). All secondary antibodies were used at a 1:1,000 dilution. Where indicated, lipids were co-stained by adding HCS LipidTOX Deep Red Neutral Lipid Stain 637/655 (1:1,000), ThermoFisher Scientific H34477) to secondary antibody solution. Cells were washed five times with PBS in an automated plate washer prior to imaging. For fixed-cell timecourse experiments, approximately 7,000 wildtype or dual-reporter OP9 cells were used to calculate mean values at each timepoint for each technical replicate.

RNAseq

siRNA targeting Pparg (# L-040712-00-0005) and Negative Control siRNA (# D-001810-10-05) were purchased from Dharmacon and transfected into OP9 cells using Lipofectamine RNAiMax (Invitrogen) according to the manufacturer's protocol. siRNA was used at a concentration of 25 nM, and the RNAiMAX/siRNA mixture was applied for 48 hours prior to the induction of differentiation. For gene expression analysis of OP9 cell samples, the cells were differentiated for 144 hours using a previously described protocol(Ahrends et al., 2014). RNA from three independent biological experiments were collected at different time points before and after induction of differentiation including (d0-d6) the extraction was completed using RNeasy Mini Kit (QIAGEN, Cat. 74104). RNA quality of all samples (n=7 time points and n=3 experiments from independent passages) was evaluated by both Nanodrop for (A260/280 >2) and Bioanalyzer 2100 High Sensitivity RNA Analysis chips (Agilent, Cat. 5067-1513) which displayed intact RNA integrity (RIN >9). mRNA samples were concentrated to ≤ 5 μl by MinElute column (QIAGEN, Cat. 74204). For generation of RNA-seq libraries, polyadenylated mRNA was isolated from 300 ng of total RNA by incubation with oligo-DT attached magnetic beads and followed by strand-specific library preparation using the TruSeq Stranded mRNA Library Preparation kit (Ilumina, Cat. 20020595). Briefly, isolated polyadenylated mRNA was fragmented using divalent cations under elevated temperature and 1st and 2nd strands DNA were synthesized using SuperScript II Reverse Transcriptase (provided with Ilumina kit). A-tailing and adapter ligation was performed according to the manufacturer's protocol; the resulting dsDNA was enriched in a PCR reaction based on predetermined CT values and cleaned using AMPure XP beads (provided with Ilumina kit). Concentrations of enriched dsDNA fragments with specific adapters were determined and base pair average size as well as library integrity were analyzed using the Bioanalyzer DNA High Sensitivity chips (Agilent, Cat. 5067-4626). Samples were pooled and sequenced on the Illumina NextSeq

500/550 High Output platform (Illumina, FC-404-2002) up to 18 samples per lane with 1% PhiX spike as a control.

The read quality of the raw FASTQ files was checked with FastQC(Andrews and Babraham Bioinformatics, 2010) (v0.11.7). Next, reads were pseudo-aligned to the mouse reference transcriptome (Mus_musculus.GRCm38.cdna) using Kallisto(Bray et al., 2016) (v0.44.0) with the quantification algorithm enabled, the number of bootstraps set to 100, and run in paired-end mode. The Kallisto output files were read into R using Sleuth, and the transcripts per million (TPM), a measurement of the proportion of transcripts in the RNA pool, was used for downstream differential expression analysis(Pimentel et al., 2017).

Measuring protein decay rates using cycloheximide

Protein decay rates were quantified as previously described(Bahrami-Nejad et al., 2018). Briefly 10,000 OP9 cells were seeded in 96-well plates) one plate for each timepoint. Cells were induced to differentiate with DMI for 24 hours. Cyclohexamide was added to the media at a final concentration of 30 μM. Cells were fixed and stained at different times after addition of cyclohexamide, and immunofluorescence was used to quantify protein concentration. Half-lives were obtained by fitting first order exponential decay curves to the data.

Fluorescent imaging

Imaging was conducted using an ImageXpress MicroXL (Molecular Devices, USA) with a 10X Plan Apo 0.45 NA objective. Live fluorescent imaging was conducted at 37°C with 5% CO_2. A camera bin of 2x2 was used for all imaging condition. Cells were plated in optically clear 96-well plates: plastic-bottom plates (Costar, #3904) for fixed imaging or glass-bottom μ-Plate (Ibidi, #89626) for live imaging. Living cells were imaged in FluoroBrite DMEM media (Invitrogen) with 10% FBS, 1% Penicillin/Streptomycin and insulin to reduce background fluorescence. Images were taken every 12 min in different fluorescent channels: CFP, YFP and/or RFP. Total light exposure time was kept less than 700 ms for each time point. Four, non-overlapping sites in each well were imaged. Cell culture media were changed at least every 48h.

Imaging data processing

Data processing of fluorescent images was conducted in MATLAB R2016a (MathWorks). Unless stated otherwise, fluorescent imaging data were obtained by automated image segmentation, tracking and measurement using the MACKtrack package for MATLAB. Quantification of PPARG- and CEBPA-positive cells in fixed samples was based on quantification of mean fluorescence signal over nuclei.

Cells were scored as PPARG- and CEBPA-positive if the marker expression level was above a preset cut-off determined by the bimodal expression at the end of the experiment.

For live imaging data of OP9 cells, the CFP channel capturing H2B-mTurqoise fluorescence was used for nuclear segmentation and cell tracking. Obtained single-cell traces were filtered to removed incomplete or mistracked traces according to the following criteria: cells absent within 6 hours of the endpoint, cell traces that started more than 4 hours after the first timepoint, cells that had large increase or decrease in PPARG intensity normalized to the previous timepoint, cells where H2B drops did not match drops in the geminin sensor. If cells were binned according to their PPARG expression, cells were binned based on their mean nuclear PPARG expression at the described timepoints.

The percent of cells in the S/G2/M phases at each time point is calculated by counting the cells that expressed the geminin reporter during the 96-hour differentiation period divided by the total number of cells. The percent of PPARG high cells was assessed by counting cells that above the PPARG threshold at that time point and dividing by the total number of cells at that time point.

Estimating a differentiation commitment point

PPARG values at the end of a differentiation experiment typically exhibit a bimodal distribution. In order to estimate a commitment point, PPARG values at the last frame of the experiment was fit to a 2 component gaussian mixture model. Cells were then classified as either differentiated or undifferentiated based on whether they more closely associated with the high or low component of the mixture model, respectively. The commitment point was then assessed as the value of PPARG at the 48-hour time point, before the stimuli was removed, that predicted the final differentiation classification with a false positive rate of less that 5%. In experiments where multiple conditions are present, the gaussian mixture model was only fitted to the negative control and the commitment point was selected based on the negative control model and applied to all other conditions in the same experiment.

Statistics

Unless specified otherwise, data are expressed as mean +/- standard error of the mean (S.E.M). Live traces are expressed as median +/- interquartile range (25th-75th percentiles). For histograms with a y-axis labeled “Fraction of Cells,” each histogram (not each plot) is normalized to the total number of cells in the population of that histogram such that all bars in the histogram add to 1. Representative results are representative of at least two independent experiments.

Data availability

All relevant data from this manuscript are available upon request.

REFERENCES

Ahrends, R., Ota, A., Kovary, K.M., Kudo, T., Park, B.O., and Teruel, M.N. (2014). Controlling low rates of cell differentiation through noise and ultrahigh feedback. Science *344*, 1384–1389.

Andrews, S., and Babraham Bioinformatics (2010). FastQC: A quality control tool for high throughput sequence data. Manual doi:citeulike-article-id:11583827.

Aragona, M., Dekoninck, S., Rulands, S., Lenglez, S., Mascré, G., Simons, B.D., and Blanpain, C. (2017). Defining stem cell dynamics and migration during wound healing in mouse skin epidermis. Nat. Commun. *8*, 14684.

Bahrami-Nejad, Z., Zhao, M.L., Tholen, S., Hunerdosse, D., Tkach, K.E., van Schie, S., Chung, M., and Teruel, M.N. (2018). A Transcriptional Circuit Filters Oscillating Circadian Hormonal Inputs to Regulate Fat Cell Differentiation. Cell Metab. *27*, 854-868.e8.

Baonza, A., and Freeman, M. (2005). Control of cell proliferation in the Drosophila eye by notch signaling. Dev. Cell *8*, 529–539.

Blais, A., Tsikitis, M., Acosta-Alvear, D., Sharan, R., Kluger, Y., and Dynlacht, B.D. (2005). An initial blueprint for myogenic differentiation. Genes Dev. *19*, 553–569.

Bray, N.L., Pimentel, H., Melsted, P., and Pachter, L. (2016). Near-optimal probabilistic RNA-seq quantification. Nat. Biotechnol. *34*, 525–527.

Buttitta, L.A., and Edgar, B.A. (2007). Mechanisms controlling cell cycle exit upon terminal differentiation. Curr. Opin. Cell Biol. *19*, 697–704.

Buttitta, L.A., Katzaroff, A.J., Perez, C.L., de la Cruz, A., and Edgar, B.A. (2007). A Double-Assurance Mechanism Controls Cell Cycle Exit upon Terminal Differentiation in Drosophila. Dev. Cell *12*, 631–643.

Cappell, S.D., Chung, M., Jaimovich, A., Spencer, S.L., and Meyer, T. (2016). Irreversible APCCdh1 Inactivation Underlies the Point of No Return for Cell-Cycle Entry. Cell *166*, 167–180.

Clayton, E., Doupé, D.P., Klein, A.M., Winton, D.J., Simons, B.D., and Jones, P.H. (2007). A single type of progenitor cell maintains normal epidermis. Nature *446*, 185–189.

Fajas, L., Landsberg, R.L., Huss-garcia, Y., Sardet, C., Lees, J.A., Auwerx, J., Illkirch, F.-, and Strasbourg, C.U. De (2002). E2Fs Regulate Adipocyte Differentiation. Dev. Cell, *3*, 39–49.

Farmer, S.R. (2006). Transcriptional control of adipocyte formation. Cell Metab. *4*, 263–273.
Fu, M., Rao, M., Bouras, T., Wang, C., Wu, K., Zhang, X., Li, Z., Yao, T.P., and Pestell, R.G. (2005). Cyclin D1 inhibits peroxisome proliferator-activated receptor γ-mediated adipogenesis through histone deacetylase recruitment. J. Biol. Chem. *280*, 16934–16941.

Ghaben, A.L., and Scherer, P.E. (2019). Adipogenesis and metabolic health. Nat. Rev. Mol. Cell Biol. *20*, 242–258.

Guo, K., Wang, J., Andrés, V., Smith, R.C., and Walsh, K. (1995). MyoD-induced expression of p21 inhibits cyclin-dependent kinase activity upon myocyte terminal differentiation. Mol. Cell. Biol. *15*, 3823–3829.

Halevy, O., Novitch, B.G., Spicer, D.B., Skapek, S.X., Rhee, J., Hannon, G.J., Beach, D., and Lassar, A.B. (1995). Correlation of terminal cell cycle arrest of skeletal muscle with induction of p21 by MyoD.

Science *267*, 1018–1021.

Han, S., Sidell, N., FIsher, P., and Roman, J. (2004). Up-regulation of p21 Gene Expression by Peroxisome Proliferator-Activated Receptor in Human Lung Carcinoma Cells. Clin. Cancer Res. *10*, 1911–1919.

Harris, T.E., Albrecht, J.H., Nakanishi, M., and Darlington, G.J. (2001). CCAAT/Enhancer-binding Protein-alpha Cooperates with p21 to Inhibit Cyclin-dependent Kinase-2 Activity and Induces Growth Arrest Independent of DNA Binding. J. Biol. Chem. *276*, 29200–29209.

Hsu, Y.-C., Li, L., and Fuchs, E. (2014). Transit-amplifying cells orchestrate stem cell activity and tissue regeneration. Cell *157*, 935–949.

Insco, M.L., Leon, A., Tam, C.H., McKearin, D.M., and Fuller, M.T. (2009). Accumulation of a differentiation regulator specifies transit amplifying division number in an adult stem cell lineage. Proc. Natl. Acad. Sci. U. S. A. *106*, 22311–22316.

Jascur, T., Brickner, H., Salles-Passador, I., Barbier, V., El Khissiin, A., Smith, B., Fotedar, R., and Fotedar, A. (2005). Regulation of p21WAF1/CIP1 Stability by WISp39, a Hsp90 Binding TPR Protein. Mol. Cell *17*, 237–249.

Jeffery, E., Church, C.D., Holtrup, B., Colman, L., and Rodeheffer, M.S. (2015). Rapid depot-specific activation of adipocyte precursor cells at the onset of obesity. Nat. Cell Biol. *17*, 376–385.

Jones, P.H., Simons, B.D., and Watt, F.M. (2007). Sic Transit Gloria: Farewell to the Epidermal Transit Amplifying Cell? Cell Stem Cell *1*, 371–381.

Lange, C., Huttner, W.B., and Calegari, F. (2009). Cdk4/CyclinD1 Overexpression in Neural Stem Cells Shortens G1, Delays Neurogenesis, and Promotes the Generation and Expansion of Basal Progenitors. Cell Stem Cell *5*, 320–331.

Naaz, A., Holsberger, D.R., Iwamoto, G.A., Nelson, A., Kiyokawa, H., and Cooke, P.S. (2004). Loss of cyclin-dependent kinase inhibitors produces adipocyte hyperplasia and obesity. FASEB J. *15*, 1–15.

Park, B.O., Ahrends, R., and Teruel, M.N. (2012). Consecutive positive feedback loops create a bistable switch that controls preadipocyte-to-adipocyte conversion. Cell Rep. *2*, 976–990.

Parker, S., Eichele, G., Zhang, P., Rawls, A., Sands, A., Bradley, A., Olson, E., Harper, J., Elledge, S., Rawls, A., et al. (2006). p53-independent expression of p21Cip1 in muscle and other terminally differentiating cells. Science *267*, 1024–1027.

Pimentel, H., Bray, N.L., Puente, S., Melsted, P., and Pachter, L. (2017). Differential analysis of RNA-seq incorporating quantification uncertainty. Nat. Methods *14*, 687–690.

Rosen, E.D., and Spiegelman, B.M. (2014). What we talk about when we talk about fat. Cell *156*, 20–44.

Ruijtenberg, S., and van den Heuvel, S. (2016). Coordinating cell proliferation and differentiation: Antagonism between cell cycle regulators and cell type-specific gene expression. Cell Cycle *15*, 196–212.

Ruijtenberg, S., van den Heuvel, S., and Van Den Heuvel, S. (2015). G1/S Inhibitors and the SWI/SNF Complex Control Cell-Cycle Exit during Muscle Differentiation. Cell *162*, 300–313.

Sabatino, L., Fucci, A., Pancione, M., Carafa, V., Nebbioso, A., Pistore, C., Babbio, F., Votino, C.,

Laudanna, C., Ceccarelli, M., et al. (2012). UHRF1 coordinates peroxisome proliferator activated receptor gamma (PPARG) epigenetic silencing and mediates colorectal cancer progression. Oncogene *31*, 5061–5072.

Sakaue-Sawano, A., Kurokawa, H., Morimura, T., Hanyu, A., Hama, H., Osawa, H., Kashiwagi, S., Fukami, K., Miyata, T., Miyoshi, H., et al. (2008). Visualizing spatiotemporal dynamics of multicellular cell-cycle progression. Cell *132*, 487–498.

Spencer, S.L., Cappell, S.D., Tsai, F.C., Overton, K.W., Wang, C.L., and Meyer, T. (2013). The proliferation-quiescence decision is controlled by a bifurcation in CDK2 activity at mitotic exit. Cell *155*, 369–383.

Tang, Q., Otto, T.C., and Lane, M.D. (2003). Mitotic clonal expansion: a synchronous process required for adipogenesis. Proc. Natl. Acad. Sci. U. S. A. *100*, 44–49.

Umek, R.M., Friedman, A.D., and McKnight, S.L. (1991). CCAAT-enhancer binding protein: a component of a differentiation switch. Science *251*, 288–292.

Wolins, N.E., Quaynor, B.K., Skinner, J.R., Tzekov, A., Park, C., Choi, K., and Bickel, P.E. (2006). OP9 mouse stromal cells rapidly differentiate into adipocytes: characterization of a useful new model of adipogenesis. J. Lipid Res. *47*, 450–460.

Wu, Z., Rosen, E.D., Brun, R., Hauser, S., Adelmant, G., Troy, A.E., McKeon, C., Darlington, G.J., and Spiegelman, B.M. (1999). Cross-Regulation of C/EBPα and PPARγ Controls the Transcriptional Pathway of Adipogenesis and Insulin Sensitivity. Mol. Cell *3*, 151–158.

Yang, H.W., Chung, M., Kudo, T., and Meyer, T. (2017). Competing memories of mitogen and p53 signalling control cell-cycle entry. Nature *549*, 404–408.

Zalc, A., Hayashi, S., Auradé, F., Bröhl, D., Chang, T., Mademtzoglou, D., Mourikis, P., Yao, Z., Cao, Y., Birchmeier, C., et al. (2014). Antagonistic regulation of p57 kip2 by Hes/Hey downstream of Notch signaling and muscle regulatory factors regulates skeletal muscle growth arrest. Development *141*, 2780–2790.

Zaragoza, K., Begay, V., Schuetz, A., Heinemann, U., and Leutz, A. (2010). Repression of Transcriptional Activity of C/EBP by E2F-Dimerization Partner Complexes. Mol. Cell. Biol. *30*, 2293–2304.

AUTHOR CONTRIBUTIONS

M.L.Z. and M.N.T. conceived experiments. M.L.Z., K.K., A.R., and Z.B. performed experiments and analyzed data. M.L.Z. and B.T. wrote the image analysis scripts. M.L.Z. and M.N.T wrote the paper with input from all authors.

ACKNOWLEDGEMENTS

This work was supported by National Institutes of Health RO1-DK101743, RO1-DK106241, P50-GM107615, a Stanford BioX Seed Grant, and a Stanford Diabetes Research Center Seed Grant (to M.N.T.), NIH F32 Postdoctoral Fellowship 5F32DK114981-02 (to B.T.), and T32-NIH T2HG00044 and NIH F31 Predoctoral Fellowship 1F31DK112570-01A1 (to M.L.Z.). The authors would like to thank Tobias Meyer, Peter Jackson, Takamasu Kudo, Antoine Zalc, Lindsey Pack (Stanford), Steve Cappell (NIH), and members of Teruel lab for helpful discussions and critical reading of the manuscript.

FIGURE LEGENDS

Figure 1. Measurement of the precise time when cells irreversibly commit to differentiate based on live single-cell analysis of endogenous expression levels of PPARG.

(A) Images of cells expressing endogenous citrine-PPARG that were differentiated using the standard 96-hour DMI protocol. Scale bar, 50 μm.

(B) Results of a typical experiment in which thousands of single cells were stimulated to differentiate. Thirty single-cell traces are shown as examples. Representative of 4 independent experiments.

(C) Scatter plot using data from (B) showing PPARG levels for each cell at 48 hours, just before the DMI stimulus was removed, and at 96 hours. Dashed black line represents the PPARG threshold (see Methods). Cells were defined as differentiated (blue) or undifferentiated (orange) by whether their PPARG levels were in the high or low intensity distributions, respectively.

(D) Citrine-PPARG cells were differentiated using the DMI protocol, and immunocytochemistry was performed at 96 hours for adipocyte markers (for each scatter plot: n > 4000 cells, representative of 2 independent experiments).

(E) The timecourses from (B) were split into equal-width bins by their PPARG values at 0, 24, 48, and 72 hours. The fraction of differentiated cells represents the number cells that crossed the PPARG threshold at the end of the experiment divided by the number of cells in the bin.

(F) Differentiating cells from (B) were computationally aligned so that the zero timepoint represents the time when the cell crossed the PPARG threshold. Plot shows 5 representative single cell traces, the median (solid black line), and the 5th-95th percentile (shaded region).

(G) PPARG timecourses from the cells that differentiated after 96 hours in (D) were computationally aligned as in (F) and plotted (blue curves). At each aligned time point, the Pearson correlation coefficient between the aligned PPARG values and the endpoint immunofluorescence values for adipocyte markers was calculated (red curves). As a comparison, PPARG values for the Glut4 panel were aligned to a randomized PPARG threshold crossing point. The randomized crossing point was generated by scrambling the vector of measured threshold points for each cell so that each threshold point is matched with different cell.

(B-F) The dotted line represents the calculated PPARG threshold for that experiment.

Figure 2. Development of a system to measure timecourses of cell cycle phases and terminal cell differentiation dynamics simultaneously in thousands of individual cells.

(A) Dual-reporter cells were made by stably expressing H2B-mTurquoise(CFP) and geminin-degron-mCherry(RFP). Data from a representative single cell entering the cell cycle is shown. Anaphase is shown both by a split in the H2B-mTurquoise signal (top images) and by a sharp drop in geminin signal (bottom timecourse). White outlines mark the position of nuclei in cells after anaphase. Scale bar, 20 μm.

(B) Dual-reporter cells were stimulated to differentiate using the standard adipogenic protocol, DMI. The timepoints at which mitosis occurred were determined by using the split in H2B signal (black open circles). Representative of 4 independent experiments.

(C) Comparison of the number of observed mitotic events that occurred in cells that were differentiated at the end of the 96-hour experiment in (B) versus cells that remained undifferentiated.

(D) Examples of PPARG (blue) and geminin-degron (red) timecourses obtained in the same single cell. The yellow dot in each plot marks the time at which that cell reached the PPARG threshold and

irreversibly committed to the differentiated state.
(E) Histogram of the difference between the time when the PPARG threshold is crossed and when mitosis last occurred for each cell in the experiment shown in (B). The PPARG threshold is reached on average ~14 hours after the last mitosis is completed. Negative values indicate cells that reached the PPARG threshold before the last mitosis was completed.
(F) A CDK2 sensor (orange trace) was added to the PPARG/geminin-degron dual-reporter cells. The resulting triple-reporter cells were differentiated using the standard DMI protocol, and representative timecourses are shown. The yellow dot in each plot marks the time at which that cell reached the PPARG threshold and irreversibly committed to the differentiated state. Representative of 2 independent experiments.
(G) Scatter plot showing the CDK2 activity versus PPARG level in each single cell at every time point. The red dashed line represents the PPARG threshold.

Figure 3. Adipogenic stimuli initiate a competition between proliferation and differentiation during a gradually extending G1 phase.
(A) Comparison of the time to commit to the next cell cycle (marked by upregulation of geminin) versus time to commit to differentiation in cells that underwent 2-3 mitoses before differentiating. *Right,* Schematic showing that the end of the second-to-last mitosis is used as the starting reference time for each cell. *Left,* histograms comparing the two times measured in the same cell (data from Figure 2B, n > 4000 cells, representative of 4 replicates).
(B) Schematic showing which G1-periods were compared in (C).
(C) *Right,* Histograms of the durations of the 1st and 2nd G1-periods in cells from (A) that have undergone at least 3 divisions. *Left,* Histogram of the difference between $G1_1$ and $G1_2$ for each cell.
(D) Plot of G1 duration versus how long a cell had been exposed to the adipogenic (DMI) stimulus at the start of G1 for each cell from (A). Red line marks average G1 duration of all cells.
(E) Timecourses from (A) were categorized into 9 bins based on time of last mitosis. The geminin peak for each bin is plotted to illustrate when the last mitosis occurred relative to addition of the adipogenic (DMI) stimulus.
(F) *Left,* Plot of binned cells from (E) showing the average time spent in G1 versus the percent of cells in that bin that were PPARG high. *Right,* Plot showing the average time of the last mitosis versus the average time it took for cells in that bin to increase PPARG levels to the differentiation commitment point.
(G) Differentiated cells from (E) were separated into four groups based on when they last exited mitosis. The traces were aligned by the last mitosis frame. The median PPARG levels were plotted for each group (dark line). Shaded region represents the 95th confidence interval.
(H) Aligned traces of cells from (E) that exited the cell cycle 24-48 hours after addition of the adipogenic (DMI) stimulus.
(I) Schematic illustrating the concept of a competition during an extended G1 between cells reaching the commitment point for differentiation or entering the next cell cycle.

Figure 4. Cyclin D1 and the CDK inhibitor p21 both regulate the length of G1 phase and antagonistically regulate adipogenesis.
(A-D) Histograms show the total time spent in G1 phase for each cell trace across all cell cycles for the respective experimental condition. The percent of cells in S/G2/M phases at each time point is

calculated by counting the cells that expressed the geminin reporter during the 96-hour differentiation period divided by the total number of cells. The percent of PPARG high cells was assessed by countin the cells with PPARG levels above the threshold divided by the total number of cells at the respective timepoint. Cells were induced to differentiate with the standard DMI protocol.

(A) Dual-reporter cells were transfected with p21 or nontargeting (control) siRNAs. Representative of 3 independent experiments.

(B) Dual-reporter cells stably expressing a DHFR-p21-mCherry fusion protein were differentiated in the presence of 10 μM TMP (to increase expression of p21) or DMSO (control). Representative of 2 independent experiments.

(C) Dual-reporter cells were transfected with cyclin D1 or nontargeting (control) siRNAs. Representative of 3 independent experiments.

(D) Dual-reporter cells were differentiated in the presence of a MEK inhibitor PD0325091 (top) or in reduced serum with and without EGF (bottom). Representative of 2 independent experiments.

Figure 5. PPARG controls cell cycle activity in part by upregulating p21 expression.

(A-D) Application of the standard DMI cocktail for 48 hours was used to induce differentiation.

(A) Dual-reporter cells were transfected with PPARG or control siRNA and then stimulated to differentiate. Differentiation and cell cycle progression were assessed in the same manner as in Figure 4A. Representative of 3 independent experiments.

(B) Wildtype OP9 cells were transfected with PPARG or nontargeting siRNA and then stimulated to differentiate. RNA samples were collected every 24 hours for 144 hours. Data is plotted as transcripts per million (TPM), and mean ± 1 SD is shown for three replicates.

(C) Dual-reporter cells were transfected with p21, p18, or nontargeting siRNAs and stimulated to differentiate. The number of cell divisions per cell is reported in the normalized histograms. Representative of 2 independent experiments.

(D) FKBPL expression under nontargeting vs PPARG knockdown were obtained from the RNA-seq data in (B). Data reported as TPM, mean ± 1 SD.

(E) Wildtype OP9 cells were transfected with FKBPL or nontargeting siRNAs, and DMI was added to initiate differentiation. Stability of p21 and PPARG were assessed by adding 30 μM cycloheximide to the media 24 hours after DMI addition and then fixing and staining for protein levels at different subsequent times. Data is plotted as mean ± 1 SD of three replicates.

(F) Wildtype OP9 cells were stimulated to differentiate by addition of 1 μM rosiglitazone. p21 levels were measured by fixing and staining cells at subsequent times. Data is plotted as mean (line) along with the values for each of the three replicates (points).

(G) Schematic connecting PPARG signaling with the regulation of cell cycle commitment through the regulation of p21 expression.

Figure 6. Cells crossing the PPARG threshold for differentiation become unresponsive to mitogenic stimulation and are locked into a post-mitotic state by p21.

(A) Plot showing how the fraction of cells in S/G2/M (red) or with PPARG levels higher than the threshold (blue) varies during a 96-hour differentiation timecourse induced by DMI.

(B) Citrine-PPARG and geminin levels were measured in dual-reporter cells in response to media replacement at 48 hours. Cells were separated into ten bins based on their PPARG levels at 48 hours. Plotted lines show mean values for each bin. Inset shows the geminin-degron signal between 48-96

hours. Representative of 2 independent experiments.
(C) PPARG values before serum refresh were binned from 100 to 2500 a.u. in 100 a.u. increments. The plot shows for each bin the fraction of cells with a minimum of one division (measured by a split in nuclear H2B signal, gray) and the final p21 level (black) and in response to serum refresh. The histogram shows the number of cells in each bin. The dotted black line shows the PPARG threshold for this experiment. Data from experiment in (B).
(D) PPARG, CEBPA, p21, and nontargeting siRNA were transfected into the dual-reporter cells at 48 hours after DMI addition. siRNA knockdown efficiency is shown in Figure S6. Representative of 3 independent experiments.
(E) A similar analysis as described in (B) was performed on the nontargeting and p21 knockdown conditions from (D).
(F) Left, A similar analysis as in (C) was performed on the nontargeting and p21 knockout conditions from (E). Right, the same data normalized to the first PPARG bin.
(G) Images of control and p21-knockdown cells from (D) obtained 48 hours after siRNA transfection (at 96 hours). Red arrows indicate representative multi-nucleated cells. Scale bar, 50 μm.
(H) OP9 cells were induced to differentiate with rosiglitazone. Cyclin D1, p21 and PPARG levels were assessed by immunocytochemistry. The PPARG threshold for the whole experiment (dotted black line) was calculated at the end of the 96-hour differentiation protocol. Representative of 2 independent experiments.

Figure 7. Stochastic competition between proliferation and differentiation during an extended G1 period controls the number of differentiated cells per precursor cell.
(A) Schematic of the three stages of G1-extension, in response to an adipogenic (DMI) stimulus. During the intermediate phase of G1-extension, stochastic competition between proliferation and differentiation causes cells to probabilistically exit into a differentiated or proliferating state. This phase defines how many differentiated cells are generated on average from a precursor cell.
(B) Schematic of how increased proliferation before the PPARG threshold could control the number of adipocytes.

SUPPLEMENTARY MATERIAL

- **Supplementary Video 1:** Dual-reporter OP9 cells induced to undergo adipogenesis by addition of the commonly-used DMI adipogenic stimulus. Daughter 1 (blue trace) and daughter 2 (red trace) only represent the product of the second mitosis (~58 hr) in the time trace. The outline represents the outline of nuclear segmentation based on the H2B channel. Geminin images, geminin trace (gray) and H2B are shown only for daughter 1.

- **Supplementary Video 2:** Dual-reporter OP9 cells transfected also with a CDK2 live-cell sensor induced to undergo adipogenesis by addition of the commonly-used DMI adipogenic stimulus.

- **6 Supplementary Figures**

SUPPLEMENTARY FIGURE LEGENDS

Figure S1. The PPARG derivative and integral values are poorer predictors of differentiation, Related to Figure 1.

(A) Traces from Figure 1B were smoothed using a Butterworth filter and a five-point stencil was applied to the smoothed traces to estimate the PPARG derivative at each timepoint. The PPARG derivative traces were then analyzed in a similar manner as in Figure1E. The bins range from -300 to 300 in intervals of 50.

(B) The PPARG integral at each time point was estimated using the trapz() function in MATLAB (MathWorks). The integral values were then analyzed in a similar manner as described in Figure 1E. The bins range from 0 to $5x10^5$ in intervals of 10^4. Note that both the derivative and integral are poor predictors for the final differentiated state. In the case of the derivative, the range between the lowest predicted probability and the highest predicted probability is smaller than found in Figure 1E. The integral values, although a good predictor for a single time point, suffers from the lack of consistency across timepoints, and a single integral value cannot be used to separate undifferentiated and differentiated cells for all timepoints.

(C) The analysis in Figure 1E was done for more time points that span the duration of the experiments and presented as a heatmap where rows represent a timepoint and the columns represents the PPARG bins as described in Figure 1E. The dotted line represents the estimated PPARG threshold for the experiment. The expanded analysis shows that the PPARG threshold remains stable throughout the experiment.

Figure S2. Additional validation of citrine-PPARG as a marker of differentiation commitment, Related to Figures 1 and 2.

(A) The switch from PPARG low to PPARG high occurs over a relatively short time window. Blue traces represent unaligned population medians of the PPARG abundance (top) and PPARG derivative (bottom). The red trace represents the PPARG abundance (top) and PPARG derivative (bottom) after computationally aligning all traces by the time when the PPARG threshold is crossed and is represented by the zero timepoint. The dashed lines highlight the time window around the peak in the PPARG derivative of the aligned traces and suggests that the switch between PPARG low and PPARG high states occurs over a short window of about 4 hours. All shaded regions represent the interquartile range (25th-75th percentiles).

(B) Unaligned correlations of endpoint markers of adipogenesis to PPARG over a typical 4-day DMI differentiation experiment. PPARG timecourses from the cells that differentiated after 96 hours in Figure 1D were averaged. At each time point, the Pearson correlation coefficient between the unaligned PPARG values, and the endpoint immunofluorescence values for adipocyte markers was calculated.

Figure S3. Sub confluent plating conditions increase cell division events during adipogenesis, Related to Figures 2 and 3.

(A) A comparison of the differentiation between dual-reporter cells plated at two different cell densities. Dual-reporter cells were differentiated using the standard DMI cocktail. The plot represents the fraction of cells that are considered past the PPARG threshold at each time point for both cell density conditions.

(B) A comparison of the fraction of dual-reporter cells in S/G2/M phases of the cell cycle, as assessed by the geminin degron sensor, for both plating conditions.
(C) The number of mitotic events for both plating conditions are reported in the histogram as the fraction of cells observed with a given number of mitosis events. The 15,000 cells per well plating condition represents a standard differentiation protocol and yields high rates of differentiation and relatively low cell-cycle activity. However, plating cells at a density of 5000 cells per well leads to a lower degree of differentiation and a higher degree of cell-cycle activity. The live cell experiments in this manuscript are plated at a density of 5000 cells per well.

Figure S4. Dilution through cell division does not significantly affect PPARG dynamics in differentiated cells, Related to Figures 2 and 3.
(A) PPARG dynamics in differentiated cells were compared between cells that divided two (blue) or three (red) times in the span of the experiment, as indicated by the geminin degron sensor (right). Additionally, the selected cells all completed the last mitosis at similar times. PPARG (left) and geminin degron (right) traces were computationally aligned to the last mitosis time. Bold traces represent median values and the shaded region represents the 95th confidence interval of the median.
(B) The trade-off between continued proliferation and differentiation exists even in cells that have been selected for undergoing exactly two divisions during the timespan of a 96-hour live-cell experiment.

Figure S5. Cyclin D1 levels do not change compared to p21 levels when adipogenic stimuli is applied, Related to Figure 5.
(A) Wildtype OP9 cells were stimulated to differentiate with the standard DMI protocol or with 1 μM Rosiglitazone. Control condition represents cells in the base media (MEM-α media supplemented with 10% FBS and Pen./Strep./Glutamine). At the end of 120 hours, cells were fixed with paraformaldehyde and immunostained for PPARG, Cyclin D1, and p21 levels.
(B) Validation of the cyclin D1 antibody by siRNA knockdown. Cells were transfected with non-targeting siRNA or cyclin D1 targeting siRNA for 24 hours and then fixed and stained for cyclin D1 levels, mean (bold line) and 95th confidence interval (shaded region).

Figure S6. Validation of the siRNA knockdown efficiency when cells were transfected at 48 hours after induction of adipogenesis, Related to Figure 6.
(A) Cells were transfected with siRNA 48 hours after addition of the adipogenic DMI stimulus and knockdown efficiency was assessed 48 hours later (at the end of the 96-hour long time-lapse experiment). To validate the siRNA knockdown efficiency of p21 and CEBPA, cells were fixed with paraformaldehyde and immunostained for p21 or CEBPA levels.
(B) PPARG knockdown was assessed using the live cell citrine-PPARG signal.

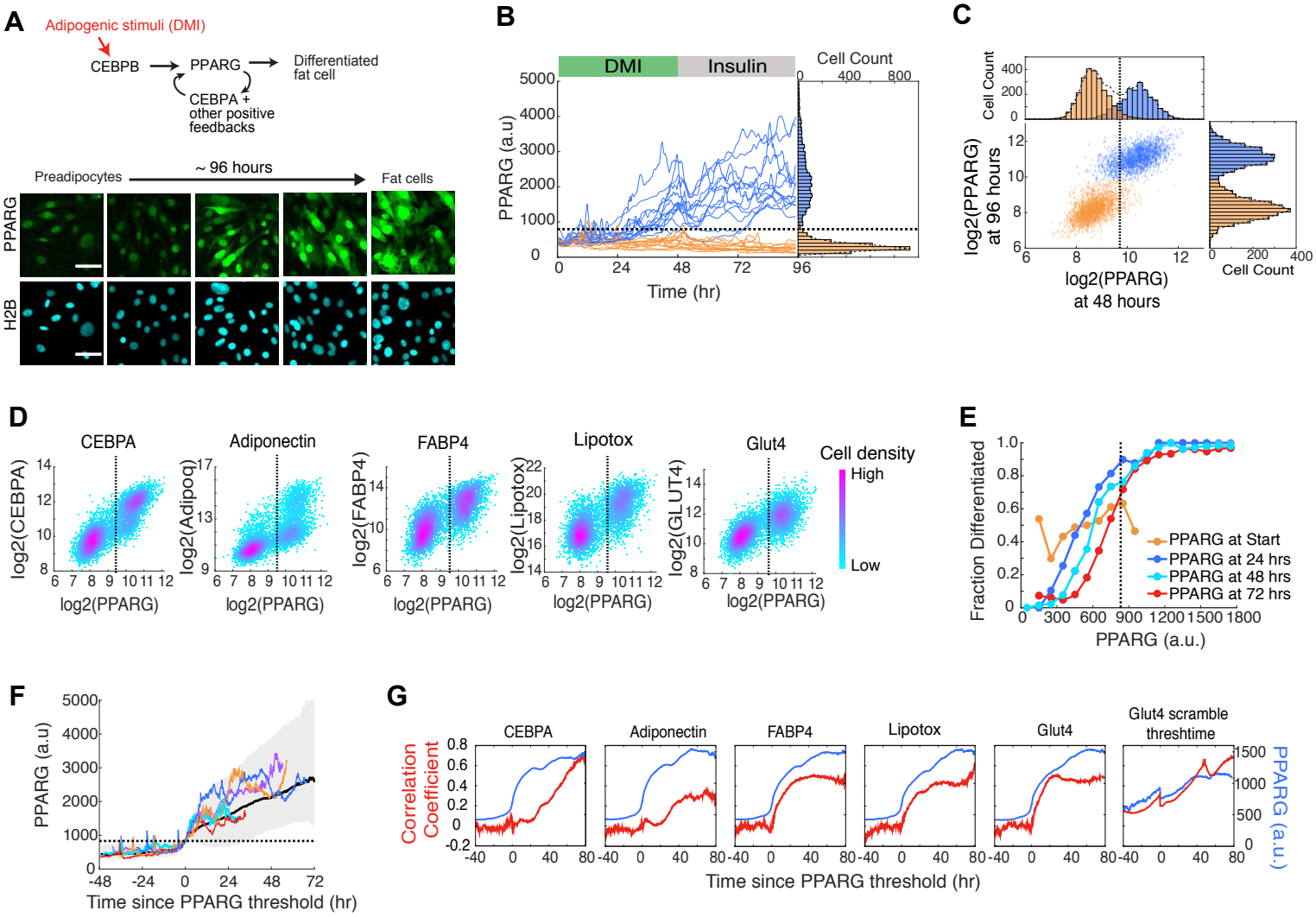

Figure 1. Measurement of the precise time when cells irreversibly commit to differentiate based on live single-cell analysis of endogenous expression levels of PPARG.

(A) Images of cells expressing endogenous citrine-PPARG that were differentiated using the standard 96-hour DMI protocol. Scale bar, 50 μm.

(B) Results of a typical experiment in which thousands of single cells were stimulated to differentiate. Thirty single-cell traces are shown as examples. Representative of 4 independent experiments.

(C) Scatter plot using data from (b) showing PPARG levels for each cell at 48 hours, just before the DMI stimulus was removed, and at 96 hours. Dashed black line represents the PPARG threshold (see Methods). Cells were defined as differentiated (blue) or undifferentiated (orange) by whether their PPARG levels were in the high or low intensity distributions, respectively.

(D) Citrine-PPARG cells were differentiated using the DMI protocol, and immunocytochemistry was performed at 96 hours for adipocyte markers (for each scatter plot: n > 4000 cells, representative of 2 independent experiments).

(E) The timecourses from (B) were split into equal-width bins by their PPARG values at 0, 24, 48, and 72 hours. The fraction of differentiated cells represents the number cells that crossed the PPARG threshold at the end of the experiment divided by the number of cells in the bin.

(F) Differentiating cells from (B) were computationally aligned so that the zero timepoint represents the time when the cell crossed the PPARG threshold. We plotted 5 representative single cell traces, the median (solid black line), and the 5th-95th percentile (shaded region).

(G) PPARG timecourses from the cells that differentiated after 96 hours in (D) were computationally aligned as in (F) and plotted (blue curves). At each aligned time point, the Pearson correlation coefficient between the aligned PPARG values and the endpoint immunofluorescence values for adipocyte markers was calculated (red curves). As a comparison, PPARG values for the Glut4 panel were aligned to a randomized PPARG threshold crossing point. The randomized crossing point was generated by scrambling the vector of measured threshold points for each cell so that each threshold point is matched with different cell.

(B-F) The dotted black line represents the calculated PPARG threshold for that experiment.

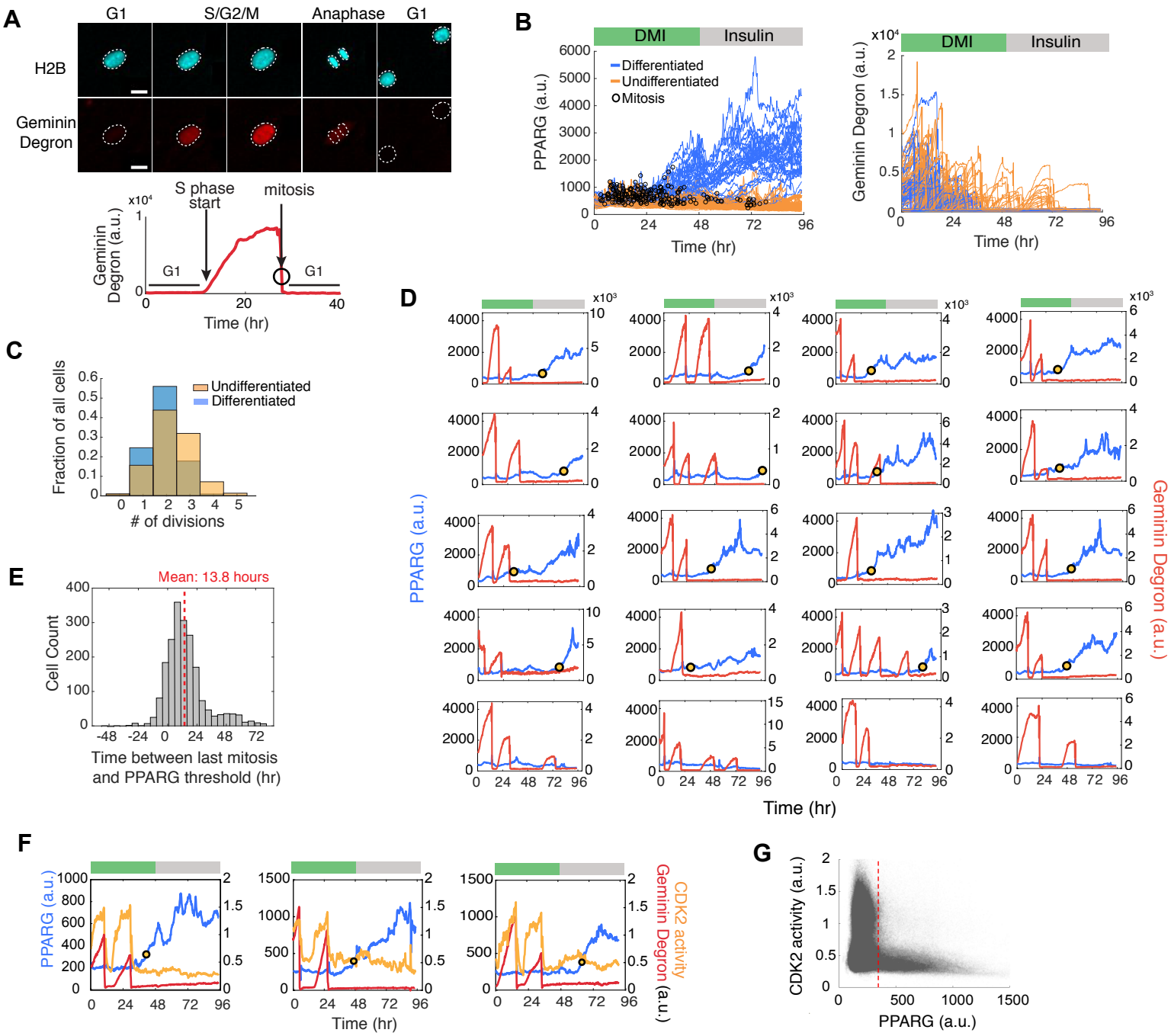

Figure 2. Development of a system to measure timecourses of cell cycle phases and terminal cell differentiation dynamics simultaneously in thousands of individual cells.

(A) Dual reporter cells were made by stably expressing H2B-mTurquoise(CFP) and geminin-degron-mCherry(RFP). Data from a representative single cell entering the cell cycle is shown. Anaphase is shown both by a split in the H2B-mTurquoise signal (top images) and by a sharp drop in geminin signal (bottom timecourse). Scale bar, 20 μm. White outlines mark the position of nuclei in cells after anaphase.

(B) The dual reporter cells allow simultaneous measurement in thousands of single cells of differentiation state using PPARG levels (left) and cell cycle state using the geminin-degron sensor (right). Cells were stimulated to differentiate with DMI using the standard adipogenic protocol. The timepoints at which mitosis occurred were determined by using the split in H2B signal (black open circles). Representative of 4 independent experiments.

(C) Comparison of the number of observed mitotic events that occurred in cells that were differentiated at the end of the 96-hour experiment in (b) versus cells that remained undifferentiated.

(D) Examples of PPARG (blue) and geminin-degron (red) timecourses obtained in the same single cell. The yellow dot in each plot marks the time at which that cell reached the PPARG threshold and irreversibly committed to the differentiated state.

(E) Histogram of the difference between the time when the PPARG threshold is crossed and when mitosis last occurred for each cell in the experiment shown in (b). The PPARG threshold is reached on average ~14 hours after the last mitosis is completed. Negative values indicate cells that reached the PPARG threshold before the last mitosis was completed.

(F) A CDK2 sensor (orange trace) was added to the PPARG/geminin-degron dual reporter cells to create triple reporter cells. Triple reporter cells were differentiated using the standard DMI protocol, and a representative trace is shown. The yellow dot represents the time when the cell reached the PPARG threshold and irreversibly committed to the differentiated state. Representative of 2 independent experiments.

(G) Scatter plot showing the CDK2 activity versus PPARG level in each single cell at every time point. The blue dashed line represents the PPARG threshold.

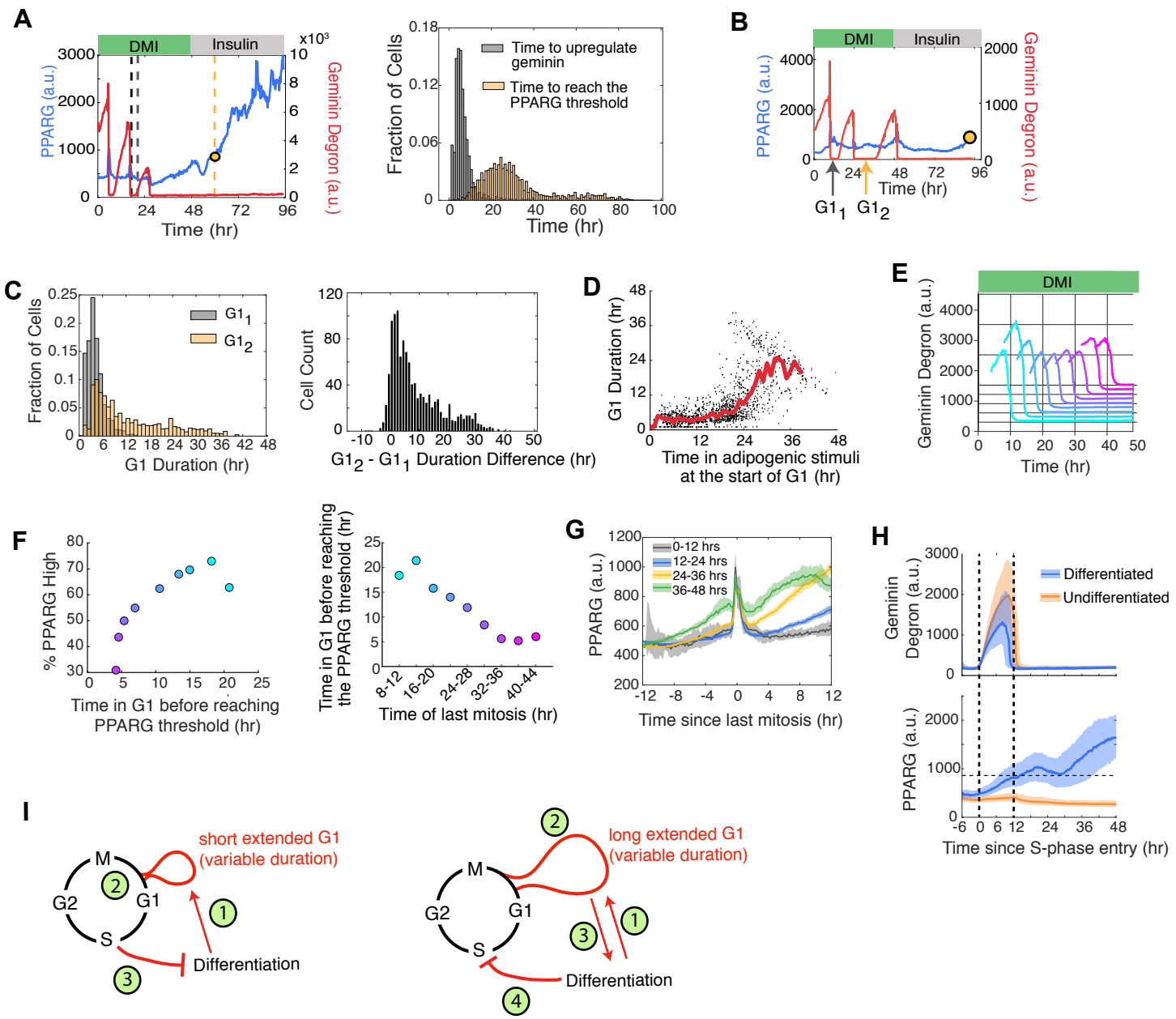

Figure 3. Adipogenic stimuli initiate a competition between proliferation and differentiation during a gradually extending G1 phase.
(A) Comparison of the time to commit to the next cell cycle (marked by upregulation of geminin) versus time to commit to differentiation in cells that underwent 2-3 mitoses before differentiating. *Right,* Schematic showing that the end of the second-to-last mitosis is used as the starting reference time for each cell. *Left,* histograms comparing the two times measured in the same cell (data from Figure 2B, n > 4000 cells, representative of 4 replicates).
(B) Schematic showing which G1-periods were compared in (C).
(C) *Right,* Histograms of the durations of the 1st and 2nd G1-periods in cells from (A) that have undergone at least 3 divisions. *Left,* Histogram of the difference between $G1_1$ and $G1_2$ for each cell.
(D) Plot of G1 duration versus how long a cell had been exposed to the adipogenic (DMI) stimulus at the start of G1 for each cell from (A). Red line marks average G1 duration of all cells.
(E) Timecourses from (A) were categorized into 9 bins based on time of last mitosis. The geminin peak for each bin is plotted to illustrate when the last mitosis occurred relative to addition of the adipogenic (DMI) stimulus.
(F) Left, Plot of binned cells from (E) showing the average time spent in G1 versus the percent of cells in that bin that were PPARG high. Right, Plot showing the average time of the last mitosis versus the average time it took for cells in that bin to increase PPARG levels to the differentiation commitment point.
(G) Differentiated cells from (E) were separated into four groups based on when they last exited mitosis. The traces were aligned by the last mitosis frame. The median PPARG levels were plotted for each group (dark line). Shaded region represents the 95th confidence interval.
(H) Aligned traces of cells from (E) that exited the cell cycle 24-48 hours after addition of the adipogenic (DMI) stimulus.
(I) Schematic illustrating the concept of a competition during an extended G1 between cells reaching the commitment point for differentiation or entering the next cell cycle.

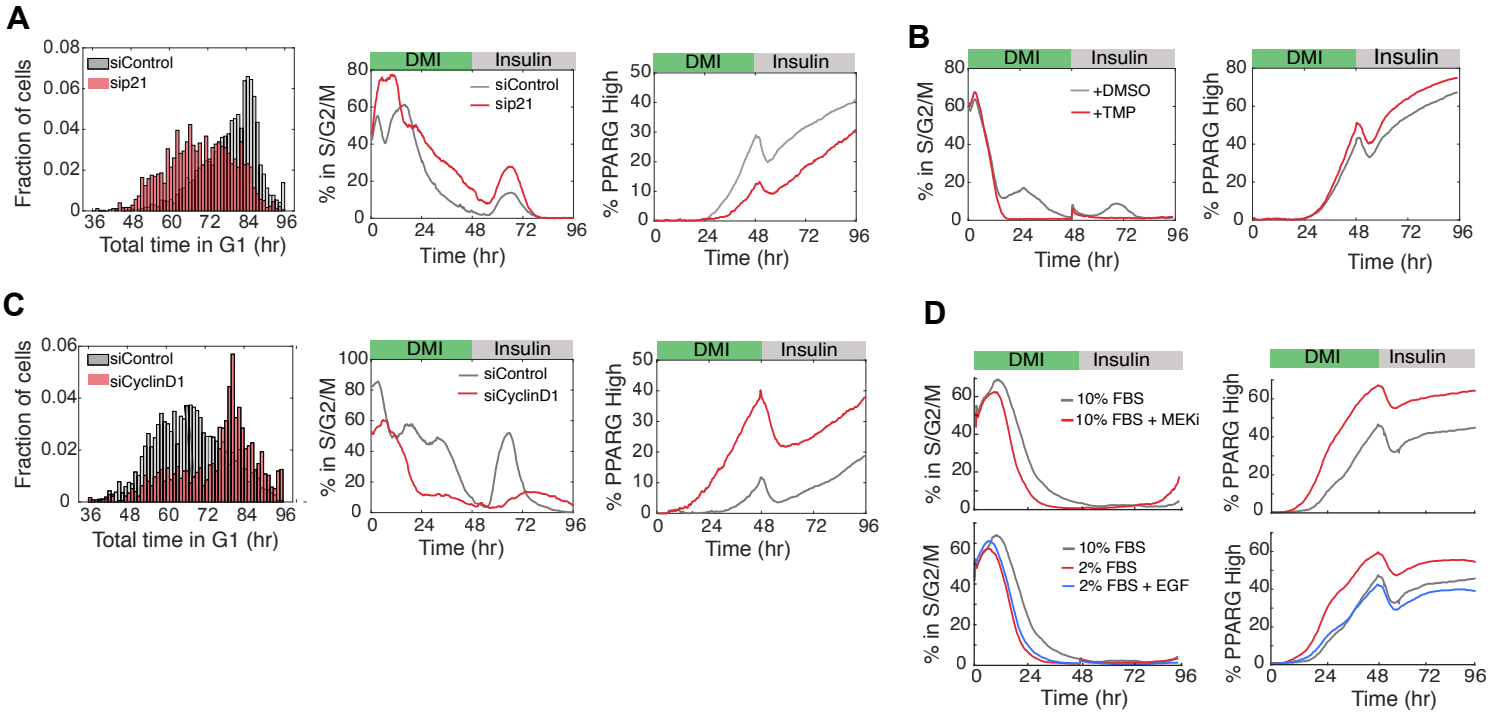

Figure 4. Cyclin D1 and the CDK inhibitor p21 both regulate the length of G1 phase and antagonistically regulate adipogenesis.

(A-D) Histograms show the total time spent in G1 phase for each cell trace across all cell cycles for the respective experimental condition. The percent of cells in S/G2/M phases at each time point is calculated by counting the cells that expressed the geminin reporter during the 96-hour differentiation period divided by the total number of cells. The percent of PPARG high cells was assessed by counting cells that above the PPARG threshold at that time point and dividing by the total number of cells at that time point. Cells were induced to differentiate with the standard DMI protocol.

(A) Dual-reporter cells were transfected with p21 or nontargeting (control) siRNAs. Representative of 3 independent experiments.

(B) Dual-reporter cells stably expressing a DHFR-p21-mCherry fusion protein were differentiated in the presence of 10 μM TMP (to increase expression of p21) or DMSO (control). Representative of 2 independent experiments.

(C) Dual-reporter cells were transfected with cyclin D1 or nontargeting (control) siRNAs. Representative of 3 independent experiments.

(D) Dual-reporter cells were differentiated in the presence of a MEK inhibitor (PD0325091, top) or in reduced serum with and without EGF (bottom). Representative of 2 independent experiments.

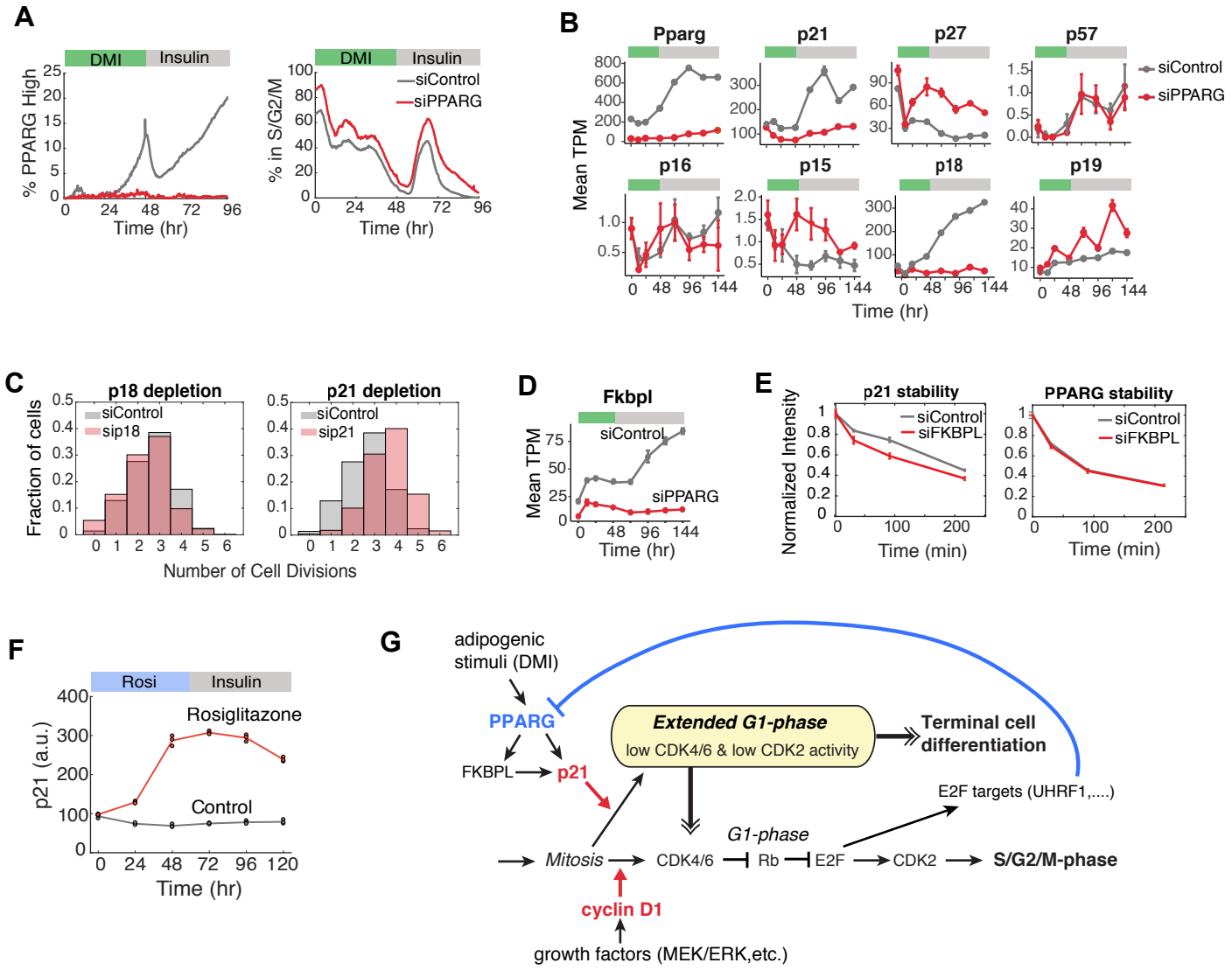

Figure 5. PPARG controls cell cycle activity in part by upregulating p21 expression.
(A-D) Application of the standard DMI cocktail for 48 hours was used to induce differentiation.
(A) Dual-reporter cells were transfected with PPARG or control siRNA and then stimulated to differentiate. Differentiation and cell cycle progression were assessed in the same manner as in Figure 4A. Representative of 3 independent experiments.
(B) Wildtype OP9 cells were transfected with PPARG or nontargeting siRNA and then stimulated to differentiate. RNA samples were collected every 24 hours for 144 hours. Data is plotted as transcripts per million (TPM), and mean ± 1 SD is shown for three replicates.
(C) Dual-reporter cells were transfected with p21, p18, or nontargeting siRNAs and stimulated to differentiate. The number of cell divisions per cell is reported in the normalized histograms. Representative of 2 independent experiments.
(D) FKBPL expression under nontargeting vs PPARG knockdown were obtained from the RNA-seq data in (B). Data reported as TPM, mean ± 1 SD.
(E) Wildtype OP9 cells were transfected with FKBPL or nontargeting siRNAs, and DMI was added to initiate differentiation. Stability of p21 and PPARG were assessed by adding 30 μM cycloheximide to the media 24 hours after DMI addition and then fixing and staining for protein levels at different subsequent times. Data is plotted as mean ± 1 SD of three replicates.
(F) Wildtype OP9 cells were stimulated to differentiate by addition of 1 μM rosiglitazone. p21 levels were measured by fixing and staining cells at subsequent times. Data is plotted as mean (line) along with the values for each of the three replicates (points).
(G) Schematic connecting PPARG signaling with the regulation of cell cycle commitment through the regulation of p21 expression.

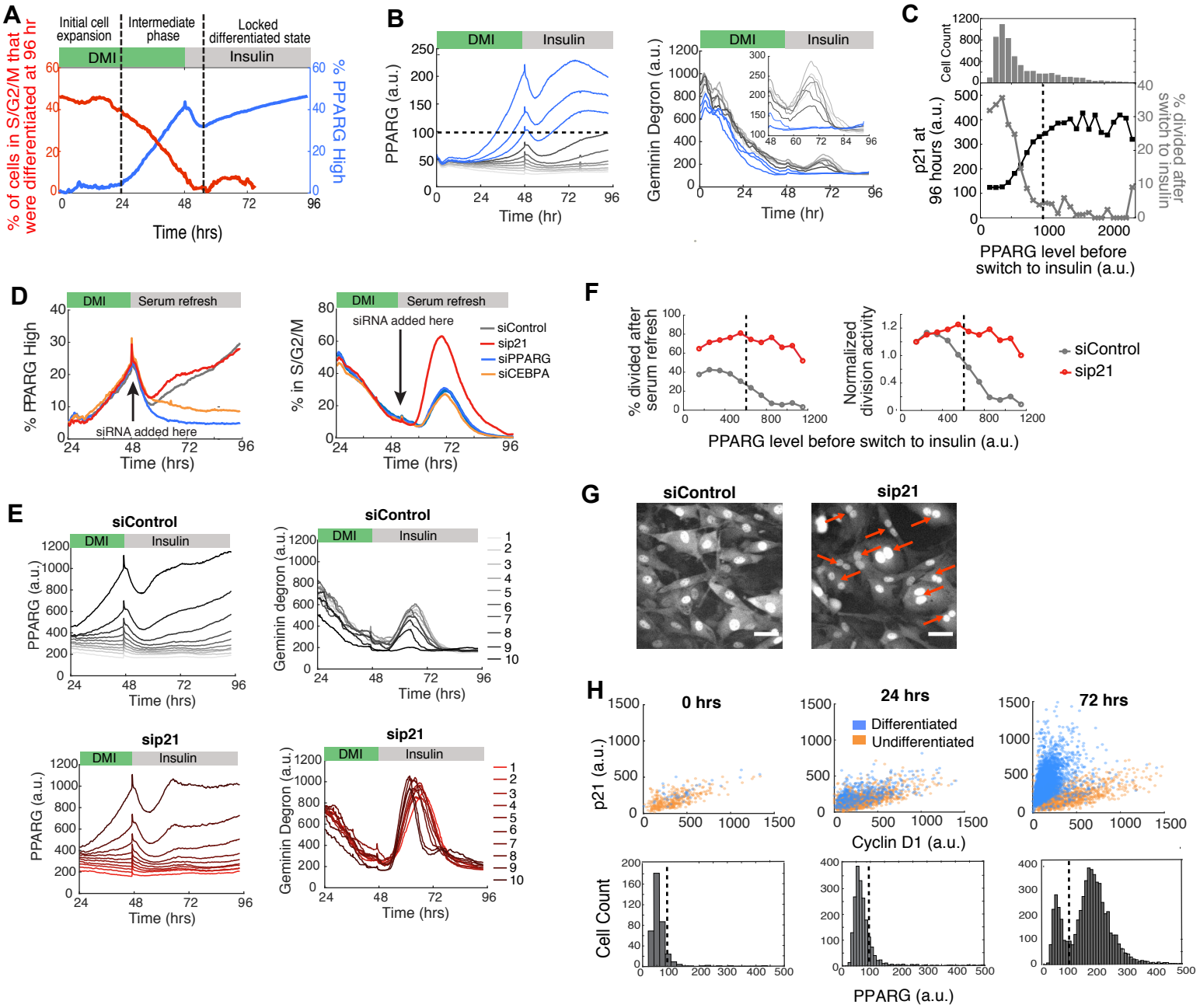

Figure 6. Cells crossing the PPARG threshold for differentiation become unresponsive to mitogenic stimulation and are locked into a post-mitotic state by p21.

(A) Plot showing how the fraction of cells in S/G2/M (red) or with PPARG levels higher than the threshold (blue) varies during a 96-hour differentiation timecourse induced by DMI.

(B) Citrine-PPARG and geminin levels were measured in dual-reporter cells in response to media replacement at 48 hours. Cells were separated into ten bins based on their PPARG levels at 48 hours. Plotted lines show mean values for each bin. Inset shows the geminin-degron signal between 48-96 hours. Representative of 2 independent experiments.

(C) PPARG values before serum refresh were binned from 100 to 2500 a.u. in 100 a.u. increments. The plot shows for each bin the fraction of cells with a minimum of one division (measured by a split in nuclear H2B signal, gray) and the final p21 level (black) and in response to serum refresh. The histogram shows the number of cells in each bin. The dotted black line shows the PPARG threshold for this experiment. Data from experiment in (B).

(D) PPARG, CEBPA, p21, and nontargeting siRNA were transfected into the dual-reporter cells at 48 hours after DMI addition. siRNA knockdown efficiency is shown in Figure S6. Representative of 3 independent experiments.

(E) A similar analysis as described in (B) was performed on the nontargeting and p21 knockdown conditions from (D).

(F) Left, A similar analysis as in (C) was performed on the nontargeting and p21 knockout conditions from (E). Right, the same data normalized to the first PPARG bin.

(G) Images of control and p21-knockdown cells from (D) obtained 48 hours after siRNA transfection (at 96 hours). Red arrows indicate representative multi-nucleated cells. Scale bar, 50 μm.

(H) OP9 cells were induced to differentiate with rosiglitazone. Cyclin D1, p21 and PPARG levels were assessed by immunocytochemistry. The PPARG threshold for the whole experiment (dotted black line) was calculated at the end of the 96-hour differentiation protocol. Representative of 2 independent experiments.

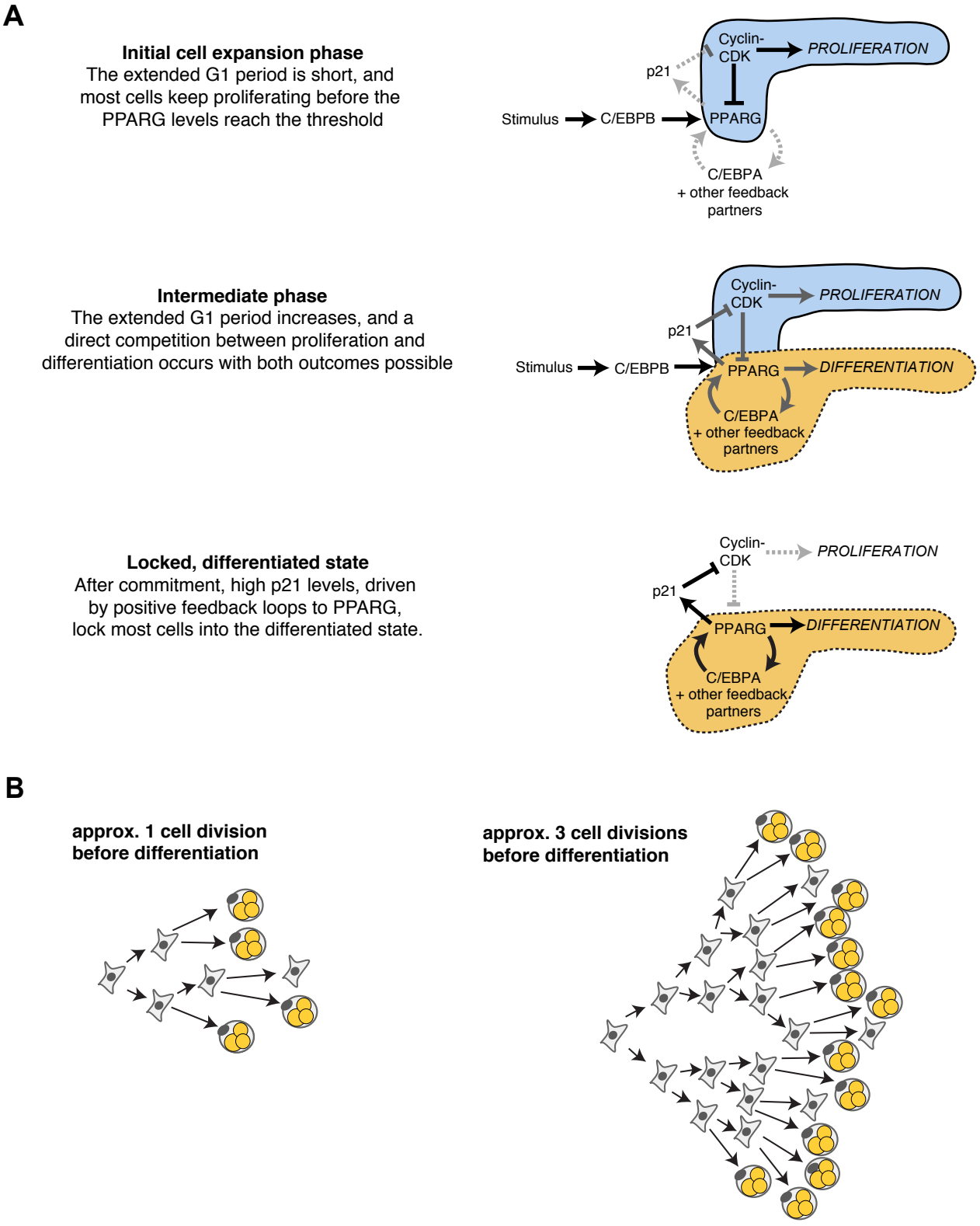

Figure 7. Stochastic competition between proliferation and differentiation in an extended G1 period controls the number of differentiated cells.
(A) Schematic of the three stages of G1-extension, in response to an adipogenic (DMI) stimulus. During the intermediate phase of G1-extension, stochastic competition between proliferation and differentiation causes cells to probabilistically exit into a differentiated or proliferating state. This phase defines how many differentiated cells are generated on average from a precursor cell.
(B) Schematic of how increased proliferation before the PPARG threshold could control the number of adipocytes.